HHS Public Access

Author manuscript

Cell Stem Cell. Author manuscript; available in PMC 2024 January 05.

Published in final edited form as:

Cell Stem Cell. 2023 January 05; 30(1): 52–68.e13. doi:10.1016/j.stem.2022.12.006.

METTL16 drives leukemogenesis and leukemia stem cell self-renewal by reprogramming BCAA metabolism

Li Han[1,2,*], **Lei Dong**[1,*], **Keith Leung**[1,*], **Zhicong Zhao**[1,5], **Yangchan Li**[1,6], **Lei Gao**[1], **Zhenhua Chen**[1], **Jianhuang Xue**[1,7], **Ying Qing**[1], **Wei Li**[1], **Sheela Pangeni Pokharel**[1], **Min Gao**[1,9], **Meiling Chen**[1,8], **Chao Shen**[1], **Brandon Tan**[1], **Andrew Small**[1], **Kitty Wang**[1], **Zheng Zhang**[1], **Xi Qin**[1], **Lu Yang**[1], **Mark Wunderlich**[10], **Bin Zhang**[3,4], **James C. Mulloy**[10], **Guido Marcucci**[3,4], **Chun-Wei Chen**[1,3], **Minjie Wei**[2,#], **Rui Su**[1,#], **Jianjun Chen**[1,3,#], **Xiaolan Deng**[1,11,#]

[1]Department of Systems Biology, Beckman Research Institute of City of Hope, Monrovia, CA 91016, USA

[2]School of Pharmacy, China Medical University, Shenyang, Liaoning 110001, China

[3]City of Hope Comprehensive Cancer Center and Gehr Family Center for Leukemia Research, City of Hope, Duarte, CA 91010, USA

[4]Department of Hematologic Malignancies Translational Science, City of Hope, Monrovia, CA 91016, USA

[5]Department of Liver Surgery, Renji Hospital, School of Medicine, Shanghai Jiao Tong University, Shanghai 200127, China

[6]Department of Radiation Oncology, The First Affiliated Hospital of Sun Yat-sen University, Guangzhou, Guangdong 510080, China

[7]Frontier Science Center for Stem Cell Research, School of Life Sciences and Technology, Tongji University, Shanghai, 200092, China

[8]Department of Hematology, Fujian Provincial Key Laboratory of Hematology, Fujian Institute of Hematology, Fujian Medical University Union Hospital, 350001 Fujian, China

[9]School of Pharmaceutical Sciences, Jiangnan University, 214122 Wuxi, China

[10]Division of Experimental Hematology and Cancer Biology, Cincinnati Children's Hospital Medical Center, Cincinnati, OH 45229, USA

[#]Correspondence: xideng@coh.org (X.D.), jianchen@coh.org (J.C.), rsu@coh.org (R.S.) and mjwei@cmu.edu.cn (M.W.).
[*]These authors contributed equally to this paper.

AUTHOR CONTRIBUTIONS

L.H., R. S., J.C. and X.D. conceived and designed the project, and supervised the research; L.H., K.L., Z.Zhao, Y.L., L.G., Z.C., Y.Q., W.L., M.G., M. C., C.S., B.T., A.S., K.W., Z.Zheng, X.Q., and X.D. performed experiments and/or data analysis; L.D. performed all the bioinformatics analysis; S.P.P., L.Y., and C.C. performed CRISPR screening; J.X. performed QQQ-MS; L.H., M. W., B.Z., J.C.M., G.M., M.W., R.S., J.C. and X.D. contributed reagents/analytic tools, patient samples, discussion, and grant support; L.H., M.W., R.S., J.C. and X.D. wrote the paper. All authors discussed the results and commented on the manuscript.

DECLARATION OF INTERESTS

J.C. is a scientific advisory board member of Race Oncology. The remaining authors declare no competing interests.

[11]Lead contact

Summary

N^6-methyladenosine (m^6A), the most prevalent internal modification in mammalian mRNAs, is involved in many pathological processes. METTL16 is a recently identified m^6A methyltransferase. However, its role in leukemia has yet to be investigated. Here we show that METTL16 is a highly essential gene for the survival of acute myeloid leukemia (AML) cells via CRISPR-Cas9 screening and experimental validation. METTL16 is aberrantly overexpressed in human AML cells, especially in leukemia stem/initiating cells (LSCs/LICs). Genetic depletion of *METTL16* dramatically suppresses AML initiation/development and maintenance and significantly attenuates LSC/LIC self-renewal, while moderately influencing normal hematopoiesis, in mice. Mechanistically, METTL16 exerts its oncogenic role by promoting expression of branched-chain amino acid (BCAA) transaminase 1 (*BCAT1*) and *BCAT2* in an m^6A-dependent manner and thereby reprogramming BCAA metabolism in AML. Collectively, our results characterize the METTL16/m^6A/BCAT1-2/BCAA axis in leukemogenesis and highlight the essential role of METTL16-mediated m^6A epitranscriptome and BCAA-metabolism reprograming in leukemogenesis and LSC/LIC maintenance.

Graphical Abstract

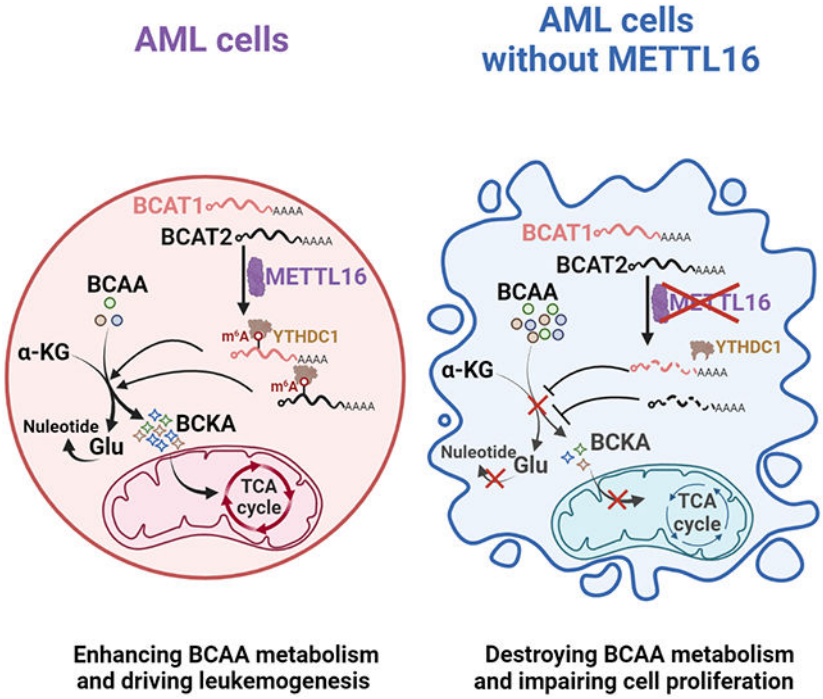

eTOC Blurb

Deng and colleagues identify METTL16, an m^6A writer, as a strong dependency in AML. METTL16 exerts its tumor-promoting role by altering the abundance of m^6A-regulated proteins, BCAT1 and BCAT2 and thereby rewiring BCAA metabolism in AML.

Keywords

METTL16; m^{6}A modification; methyltransferase; AML; leukemia stem/initiating cells (LSCs/LICs); self-renewal; BCAA metabolism; BCAT1; BCAT2

INTRODUCTION

Acute myeloid leukemia (AML) is a type of aggressive hematopoietic malignancy with clonal expansion of the immature myeloid cells and the impaired differentiation of myeloid progenitor cells.[1] AML development is highly orchestrated in a cellular hierarchy, with leukemia stem/initiating cells (LSCs/LICs) at the apex of this precise regulation. LSCs/LICs are recognized as root cause of leukemia initiation, relapse, and drug resistance.[2-5] Albeit the improvement of treatment-adapted strategies, over 70% of AML patients cannot survive over 5 years due to drug resistance and relapse.[1,6] Thus, it is critical to better understand the molecular mechanism(s) underlying leukemogenesis and LSC/LIC self-renewal, which may lead to the identification of new therapeutic targets and the development of improved therapeutics for AML treatment.

In contrast to normal hematopoietic cells, leukemia cells are notorious for their robust plasticity in response to the stressful microenvironment and acquired metabolic adaptations to support the uncontrolled proliferation, which is termed as metabolic reprogramming.[7] The cancer-associated metabolic reprogramming has profound effects on gene expression, differentiation and tumor progression, and has been recognized as an emerging hallmark of malignancy.[8,9] Recently, the branched-chain amino acid (BCAA; valine, leucine and isoleucine) metabolism has been associated with aggressiveness in various human cancers, including leukemia.[10-12] The BCAAs serve as requisite substrates for protein synthesis, replenish pools of the tricarboxylic acid (TCA) cycle intermediates, and act as a source of nitrogen for nucleotides synthesis. [13,14] Branched-chain aminotransferase isozymes, BCATs, including cytosolic BCAT1 and mitochondrial BCAT2, catalyze the reversible transamination that transfers an amino group from BCAA to α-ketoglutarate (α-KG), generating glutamate and the corresponding branched-chain α-keto acids (BCKAs). More strikingly, both the BCAT1 expression and the degradation of BCAAs are highly enriched in LSCs relative to non-LSCs, and AML is addicted to BCAA metabolism to maintain the leukemia stemness.[11] Nevertheless, how BCAA metabolism is reprogrammed in AML remains elusive.

As the most abundant internal modification in mammalian mRNA, N^6-methyladenosine (m^{6}A) fine-tunes gene expression at post-transcriptional level via regulating mRNA stability, translation efficiency, alternative splicing, and nuclear export.[15-17] Evidence is emerging that the dysregulation of m^{6}A decoration and its machinery is involved in various types of cancers, including AML.[18-29] According to current knowledge, the m^{6}A decoration in mRNA is mainly deposited by the METTL3-METTL14 methyltransferase complex (MTC; also known as m^{6}A "writer"). Both METTL3 and METTL14 have been linked to the initiation and progression of AML via an m^{6}A-dependent mechanism.[18,19,28] METTL16 was a recently identified m^{6}A methyltransferase independent from the METTL3/14

complex, which can add m^{6}A on several non-coding RNAs and one mRNA (*MAT2A*).[30-35] We very recently reported that METTL16 can also deposit m^{6}A modification to hundreds or even thousands of mRNAs.[36] However, the roles of METTL16 in AML and normal hematopoiesis have yet to be investigated.

Here we report that *METTL16* is a more essential gene than *METTL3* and *METTL14* for the survival of AML cells, and is also required for the self-renewal LSCs/LICs. METTL16 exerts its tumor-promoting role by enhancing the expression of its critical targets such as *BCAT1* and *BCAT2* in an m^{6}A-dependent manner, and thereby reprograms BCAA metabolism and promotes leukemogenesis and LSC/LIC self-renewal.

RESULTS

METTL16 is the most essential *METTL* gene for the survival of AML cells, in which it is overexpressed

Human methyltransferase like proteins (METTL) constitutes a large family characterized by the seven-β-strand methyltransferases with S-adenosyl methionine binding domains.[37] METTL proteins have been recognized or predicted to catalyze the methylation of DNA, RNA, and proteins, contributing to epigenetic or epitranscriptomic regulation of gene expression.[38,39] However, except for METTL3 and METTL14, the roles of most METTL proteins in normal physiological process and pathogenesis remain poorly understood. Analysis of the data from a genome-wide CRISPR-Cas9 knockout (KO) screening across over 800 cancer cell lines[40] revealed the stronger dependency of METTL16 in leukemias than in other cancer types (Figure 1A), along with the stronger dependency of METTL16 in AML cell lines than in non-AML leukemia cell lines (Figure 1B). Strikingly, among all the METTL members, METTL16 is the most essential one for the survival/proliferation of AML cells or all types of hematopoietic malignant cells (Figures 1C and S1A). To validate the dependency of METTL16 in AML cell survival/proliferation, we designed a small library targeting the coding regions of DNA and RNA methylation related genes and conducted CRISPR screening with Cas9 single-cell clones of AML cells (Figure 1D). Given the well-recognized oncogenic roles of METTL3 and METTL14 in AMLs,[18,19,28] we included them as positive controls; METTL4 was included as a negative control because it is not essential for the survival of any tumor cells (Figures 1C and S1A). Our CRISPR screening data demonstrated that *METTL16* indeed is a more essential gene than the other *METTL* genes for the survival of AML cells (Figure 1E). Moreover, METTL16 is aberrantly overexpressed in AML samples relative to healthy controls at both mRNA level (Figures 1F, 1G, and S1B)[20] and protein level (Figure 1H).

Consistently, our *in vitro* functional studies showed that *METTL16* KO dramatically inhibited survival/growth and promoted apoptosis and myeloid differentiation of various AML cell lines with distinct molecular and chromosomal abnormalities; such effects could be completely reversed by forced expression of sgRNA-resistant *METTL16* (Figures 1I, 1J, and S1C-S1F). Knockdown (KD) of *METTL16* by two different short hairpin RNAs (shRNAs) showed similar effects to *METTL16 KO* (Figures S1G-S1I). Taken together, our data suggest that METTL16 is essential for the proliferation, survival and undifferentiation of AML cells *in vitro*.

METTL16 is required for AML development and maintenance

To elucidate the role of METTL16 in leukemogenesis, we isolated mouse bone marrow (BM) lineage negative (Lin^-) progenitor cells, a type of hematopoietic stem/progenitor cells (HSPCs), and virally transduced them with *MLL-AF9* (MA9; a common AML fusion gene, which is resulting from t(9;11)[5]), and then conducted colony forming/replating assay (CFA) and primary BM transplantation (BMT) assay (Figure 2A and S2A). We first used a lentiviral vector-based shRNA system to knock down *Mettl16* in MLL-AF9-induced pre-leukemic cells (Figure S2A). KD of *Mettl16* significantly inhibited MA9-induced leukemic cell transformation and colony forming (Figures S2B and S2C). Through BMT assays, we showed that *Mettl16* KD dramatically blocked AML initiation and development in the recipient mice, and none of the mice within the two KD groups developed AML (Figure S2D). *Mettl16* KD also dramatically restrained the expansion and infiltration of leukemic blast cells into BM, spleen, peripheral blood (PB), liver, and spleen (Figures S2E and S2F). Furthermore, *Mettl16* KD remarkably suppressed splenomegaly (Figure S2G) and decreased white blood cell (WBC) counts (Figure S2H) in the recipient mice. To further validate the robust oncogenic function of Mettl16 in AML initiation/development, we generated *Mettl16* conditional knockout (cKO) mice by cross $Mettl16^{fl/fl}$ mice with Mx1-Cre mice (Figures S3I and S3J). The Lin^- BM progenitor cells were isolated from *Mettl16* wild-type (WT), $Mettl16^{fl/+}$;Mx1-Cre (Hetero), and $Mettl16^{fl/fl}$;Mx1-Cre (Homo) mice and then transduced with MA9 retroviruses (Figure 2A). Our serial CFA results indicated that depletion of *Mettl16* significantly suppressed the colony-forming/repopulation capacity of primary MA9 cells in a dose-dependent manner (Figures 2B and 2C). Consistently, heterozygous KO of *Mettl16* significantly delayed leukemia initiation/development, prolonged survival, suppressed the engraftment of leukemia cells, and mitigated splenomegaly of the MA9-driven primary AML models, while homozygous KO of *Mettl16* showed a much more profound anti-leukemia activity than did heterozygous KO and completely inhibited leukemogenesis (Figures 2D, 2E, and S2K). In addition to the MA9 AML model, we have also evaluated the effect of *Mettl16* cKO on the colony-forming/repopulation capacity in other common AML models, including those induced by AML1-ETO9a (AE9a)/t(8;21)[41] and PML-RARA/t(15;17). Our results demonstrated that Mettl16 KO, especially homozygous KO, dramatically suppressed colony formation/repopulation of both AE9a- and PML-RARA-bearing AML cells (Figures S2L-S2Q), implying a broad oncogenic role of METTL16 in AML.

We next evaluated the function of METTL16 in human AML maintenance and progression *in vivo* through the “human-in-mouse” xenotransplantation leukemia models with immune-deficient mice and monitored leukemia burden via bioluminescent imaging (Figure 2F). *METTL16* KO remarkably reduced the bioluminescence signals and leukemia burden, inhibited the *in vivo* engraftment of human AML cells, and substantially elongated the overall survival in the recipient mice (Figures 2G and 2H). Restoration of sgRNA-resistant form of METTL16 could totally reverse the *METTK16* KO-mediated phenotypes *in vivo* (Figures 2G-2J), indicating that the inhibitory effect of *METTL16* KO on AML progression is not an off-target effect. Similarly, shRNAs-mediated *METTL16* KD also significantly suppressed human AML maintenance and progression *in vivo*, and prolonged survival in mice (Figures 2K and 2L). Moreover, we further validated the oncogenic role of

METTL16 in AML by use of patient-derived xenograft (PDX) AML models with distinct genetic backgrounds. Similarly, *METTL16* KO remarkably impaired primary human AML progression, reduced leukemia burden, facilitated myeloid differentiation, and prolonged survival in the recipient mice (Figures 3A-3F and S3A-S3H); again, forced expression of sgRNA-resistant form of METTL16 could sufficiently reverse all these phenotypes in the PDX models (Figures 3A-3D and S3A-S3D). Collectively, our data strongly demonstrate a crucial oncogenic role of METTL16 in AML initiation, progression and maintenance.

METTL16 is critical for the self-renewal of LSCs/LICs

Via intracellular flow cytometry staining, we found that METTL16 protein level is significantly higher in primary AML patient samples than in healthy control cells; moreover, its level is significantly higher in $CD34^+$ immature AML blast cells (representing LSC/LIC population) than in $CD34^-$ AML bulk cells (Figures 3G-3I and S3I-S3K), implying that METTL16 may play a role in the self-renewal of LSCs/LICs. To determine the role of METTL16 in LSC/LIC maintenance, we first knocked down *METTL16* by shRNAs in human primary $CD34^+$ AML cells which were isolated from different AML patients (Figure S3L). *METTL16* KD significantly impaired cell growth, induced apoptosis, and suppressed the colony-forming/repopulation capacity of human primary AML cells (Figures S3M-S3O), indicating that METTL16 is required for the survival and self-renewal of human primary $CD34^+$ LSCs/LICs.

We next examined Mettl16 expression in the LSCs/LICs isolated from the BM of primary MLL-AF9-driven AML mice. We found that *Mettl16* is expressed at a significantly higher level in Lin^- LSCs /LICs than in the Lin^+ populations (Figure S3P), implying that Mettl16 likely also plays a role in the self-renewal of murine LSCs/LICs. Indeed, *Mettl16* heterozygous KO significantly decreased the populations of granulocyte-macrophage progenitors (GMP)-like LSCs in the primary MA9 AML models (Figures 3J and 3K). As *Mettl16* homozygous KO group did not have MA9 AML cell engraftment in the mice, we could not detect such GMP-like LSCs. Moreover, to investigate the role of Mettl16 in the repopulating activity of LSCs/LICs, we isolated AML cells from the primary BMT mice and virally transduced *Mettl16* shRNAs or vehicle control into the AML cells, and then transplanted them into recipient mice for secondary BMT. *Mettl16* KD almost completely abrogated the reconstitution capacity of primary AML cells and suppressed the development of AML in the secondary BMT recipient mice (Figures S3Q-S3S).

To quantitatively assess the effect of *Mettl16* depletion on LSC/LIC frequency/self-renewal, we conducted *in vitro* and *in vivo* limiting dilution assays.[5,42,43] As expected, *Mettl16* KD led to a dramatic decrease in the frequency of LSCs/LICs in murine MLL-AF9 AML model *in vitro* (Figure S3T) and *in vivo* (Figure 3L). Taken together, our data demonstrate that METTL16 plays a critical role in maintaining the self-renewal/repopulation capacity of LSCs/LICs.

METTL16 deletion moderately affects normal hematopoiesis

METTL3 and METTL14 have been reported to promote self-renewal of normal hematopoietic stem cells (HSCs),[19,28,44-47] whereas YTHDF2 (an m^6A reader) was shown

to repress HSC self-renewal.[48,49] In contrast, ALKBH5 (an m^6A eraser) was reported to be dispensable for HSC self-renewal and normal hematopoiesis.[23,29] To determine whether METTL16 is a potential safe therapeutic target for AML treatment, we sought to investigate the role of METTL16 in normal hematopoiesis. We found that METTL16 is expressed at a higher level in human umbilical cord blood (UCB)-derived $CD34^+$ HSPCs than in $CD34^-$ cells (Figures S4A and S4B). Similarly, qPCR and western blot analysis revealed that Mettl16 is also highly expressed in murine Lin^- BM progenitor cells relative to the bulk cells, Lin^+ cells, $Mac1^+$ monocytes, or $Gr1^+$ granulocytes (Figures S4C and S4D), hinting that the expression levels of Mettl16 might be decreased during myeloid differentiation. Indeed, we utilized OP9 cell-based coculture system to induce the myeloid differentiation of murine Lin^- HSPCs[28] and observed a significant reduction of Mettl16 level (Figures S4E). In addition, via intracellular flow cytometry staining, we analyzed the expression of Mettl16 at different stage of the hematopoietic differentiation hierarchy. We found that, compared to the differentiated Lin^+ cells, Mettl16 is highly expressed in HSPC compartments, including $CD150^+CD48^-Lin^-Sca1^+cKit^+$ hematopoietic stem cells (HSCs), multipotent progenitors (MPPs), primitive hematopoietic progenitors (HPC-1 and HPC-2 populations), common myeloid progenitor (CMP), granulocyte/monocyte progenitor (GMP) and megakaryocyte/erythroid progenitor (MEP) (Figure S4F). Amongst all these hematopoietic cells, Mettl16 is extremely highly expressed in HSCs.

To elucidate the function of Mettl16 in normal hematopoiesis, we utilized the *Mettl16* cKO mouse model and induced the hematology-specific *Mettl16* KO with poly(I:C) to evaluate the effects of *Mettl16* depletion on complete blood counts of PB and the frequency of functional hematopoietic lineages, including B-lymphoid ($B220^+$), T-lymphoid ($CD3^+$), myeloid ($Mac1^+Gr1^+$), erythroid ($Ter119^+$) cells in BM and spleen (Figures 4A and 4B). Albeit homozygous *Mettl16* KO moderately decreased the frequencies of white blood cell (WBC), lymphoma cell (LYM), and platelet (PLT) in the PB (Figures 4C and 4D), it had little effects on the populations of other hematopoietic cells, including granulocyte (GRA), monocyte (MONO), red blood cell (RBC), as well as hemoglobin (HGB) level in the PB (Figures 4E-4H). Homozygous *Mettl16* KO also resulted in mild changes of $B220^+$ B cells in BM and spleen, as well as $CD3^+$ T cells and $Ter119^+$ erythroid cells in spleen (Figures S4G and S4H). Heterozygous *Mettl16* KO didn't show any significant effects on normal hematopoiesis (Figures 4C-4H, S4G, and S4H). Furthermore, we determined the populations of hematopoietic progenitors in the BM. Our results showed that that homozygous *Mettl16* KO significantly decreased the HSC and MEP populations, while increased HPC-1 population, whereas heterozygous *Mettl16* KO didn't show significant effects on any of these populations (Figures 4I, 4J, and S4I). To further investigate the role of *Mettl16* in HSC self-renewal *in vivo*, we have performed *in vivo* competitive repopulation assay (Figures S4J). The BM cells from homozygous *Mettl16* KO mice showed a significantly lower reconstitution capacity compared to the WT counterpart, whereas heterozygous BM cells showed a comparable self-renewal ability to the WT cells (Figure S4K). Such data suggest that Mettl16 may play a role in maintaining normal HSC self-renewal in hematopoiesis in the competitive stress state.

We further assessed the effects of *METTL16* depletion on the proliferation and colony-forming ability of normal HSPCs. As shown in Figures 4K-4N, neither *METTL16* KD in

human CD34$^+$ HSPCs nor *Mettl16* KD in murine Lin$^-$ HSPCs impaired the growth of those normal HSPCs. *METTL16* KD or *Mettl16* KO showed a much more profound inhibitory effect on the colony-forming/repopulation ability of AML patient-derived human CD34$^+$ LSCs/LICs or murine MA9 LSCs/LICs than on that of human healthy CD34$^+$ HSPCs or murine Lin$^-$ HSPCs (Figures 4O-4R, S4L and S4M). Collectively, compared to normal HSPCs, LSCs/LICs rely more on the expression/function of METTL16.

METTL16 exerts its pathological role as an m^{6}A methyltransferase and regulates expression of a set of metabolism-associated targets in AML

To decipher the mechanism(s) by which METTL16 exerts its oncogenic role in AML, we first assessed whether the methyltransferase activity of METTL16 is required for its oncogenic role. Through knockout-rescue assays with sgRNA-resistant form of WT METTL16 and two catalytically inactive mutants (PP185/186AA and F187G) (Figure 5A), we found that restoration of WT METTL16, but not the two mutants, could substantially rescue the cell growth defect and apoptosis caused by *METTL16* KO in AML cells (Figures 5B, 5C, and S5A-S5C). Such data indicate that the oncogenic role of METTL16 fully depends on its enzymatic activity in AML.

To identify the *bona fide* targets which are responsible for the oncogenic role of METTL16 in AML, we conducted m^{6}A sequencing (m^{6}A-seq) and transcriptome-wide RNA sequencing (RNA-seq). By analysis of m^{6}A-seq data, we revealed that *METTL16* KO resulted in a significant decrease of m^{6}A abundance in 4,736 transcripts (Figure 5D). The RNA-seq was performed with three groups, including control group, *METTL16* KO group, and rescue group (*METTL16* KO plus METTL16 overexpression). Principal component analysis (PCA) and cluster analysis showed that control group and rescue group can be clustered together, separate from the *METTL16* KO group (Figures 5E). Analysis of RNA-seq data identified hundreds of differentially expressed genes (DEGs), including significantly down- and up-regulated genes upon *METTL16* KO (Figure 5F). Critically, the expression of these DEGs could be extensively reversed by forced expression of METTL16, highlighting that the expression changes of those genes were directly attributed to *METTL16* depletion (Figures 5G, 5H, S5D, and S5E). By integrative analysis of RNA-seq and m^{6}A-seq data, we found that 267 mRNA transcripts with *METTL16* KO-induced hypo-m^{6}A peaks were significantly downregulated, while 474 mRNA transcripts with *METTL16* KO-induced hypo-m^{6}A peaks were significantly upregulated (Figures 5I and S5F).

Then, we conducted GSEA pathway analysis[50] of the 267 hypo-down transcripts and the 474 hypo-up transcripts. The hypo-down transcripts were involved in multiple biological pathways related to leukemogenesis, such as valine, leucine and isoleucine (BCAA) biosynthesis, RNA polymerase II transcription, amino acid metabolism, and cell cycle; amongst them, BCAA biosynthesis was the top one pathway (Figure 5J). In contrast, the hypo-up transcripts were enriched in various other pathways (Figure S5G); among them, the activation of hematopoietic stem cell differentiation pathway might be responsible for the phenotype that *METTL16* depletion promoted myeloid differentiation of AML cells (Figures S5H and S5I). We then ranked all the enriched core genes in the top

hypo-down pathways and noticed that the most significantly down-regulated genes, such as *BCAT1*, *BCAT2,* leucyl-tRNA synthetase 1 (*LARS1*), and isoleucyl-tRNA synthetase 1 (*IARS1*), play a central role in the BCAA biosynthesis (Figures 5K and 5L). Our RNA-seq data showed that *METTL16* KO significantly inhibited expression of *BCAT1, BCAT2, LARS1,* and *IARS1,* which can be completely reversed by ectopic expression of sgRNA-resistant METTL16 (Figure 5M). Notably, our METTL16 RIP-qPCR data demonstrated that METTL16 directly bound to *BCAT1, BCAT2, LARS1,* and *IARS1* transcripts in AML cells (Figures 5N and S5J). Furthermore, we confirmed that *METTL16* KO significantly suppressed the expression of these four genes at both RNA level and protein level and restoration of METTL16 expression could completely reverse their downregulation (Figure 5O, 5P, S5K and S5L). Therefore, these four critical genes in the BCAA biosynthesis pathway appear to be direct targets of METTL16 in AML.

BCAT1 and *BCAT2* are the m^{6}A-dependent targets of METTL16 in AML

BCAAs not only can be catalyzed by specific aminoacyl-tRNA synthetases, such as LARS1 and IARS1, onto their cognate tRNAs and incorporated into proteins during mRNA translation, but also can be transaminated by BCAT1 and BCAT2 to produce their corresponding BCKAs and glutamate.[51] BCKAs can further fuel TCA cycle metabolism and oxidative phosphorylation to produce energy for cells. Thus, BCAAs can be used for both protein synthesis and energy production. Notably, in the majority of cancer cells, particularly LSCs, BCAT1 and BCAT2-mediated BCAA catabolism is the predominant reaction.[11,52] Thus, we focused on BCAT1 and BCAT2 for further mechanistic and functional studies. We first conducted gene-specific m^{6}A qPCR and validated that *METTL16* KO significantly decreased m^{6}A abundance in *BCAT1/2* mRNAs, which could be reversed by METTL16 restoration (Figure 6A). To further determine whether METTL16 can directly deposit m^{6}A in *BCAT1* and *BCAT2* transcripts, we conducted *in vitro* m^{6}A methyltransferase assays coupled with triple-quadrupole-mass spectrometer (QQQ-MS) detection (Figures 6B and S6A). As expected, METTL16 protein could directly methylate *BCAT1* and *BCAT2* mRNA *in vitro* (cell-free) (Figures 6C). In addition, our METTL16 RIP-qPCR data showed that METTL16 protein strongly bind to multiple m^{6}A-modified regions of *BCAT1/2* transcripts in human AML cells (Figures 6D and S6B-S6D), but not in human normal CD34$^+$ HSPCs (Figures S6E), indicating that METTL16 might have distinct targets between AML and healthy control cells.

We next conducted RNA stability assay and showed that *METTL16* KO significantly decreased the stability of *BCAT1* and *BCAT2* transcripts and downregulated their expression (Figures 6E, 6F and S6F). *METTL16* KO-induced downregulation of *BCAT1/2* could be rescued by ectopic expression of WT METTL16, but not the two catalytically inactive mutants (Figures 6F and S6F), indicating that METTL16-mediated m^{6}A methylation increases the stability of *BCAT1/2* mRNAs and promotes their expression in AML cells. According to current knowledge, IGF2BP proteins and YTHDC1 can recognize m^{6}A modification and stabilize the m^{6}A-modified mRNAs.[25,53,54] We knocked down the endogenous expression of *IGF2BP2* (IGF2BP1/3 levels in AML are not high enough) and *YTHDC1* in AML cells and found that *YTHDC1* KD, but not *IGF2BP2* KD, significantly decreased the stability of both *BCAT1* and *BCAT2* (Figures 6G and S6G). Moreover,

YTHDC1, but not IGF2BP2, directly interacted with *BCAT1* and *BCAT2* mRNAs (Figure 6H and S6H). As expected, *YTHDC1* KD resulted in significant decrease of *BCAT1* and *BCAT2* expression in AML cells (Figure S6I). Taken together, our results suggest that METTL16 deposits the m^6A modifications in *BCAT1* and *BCAT2* transcripts and YTHDC1 can recognize those m^6A sites and stabilize the two mRNA targets in AML.

The METTL16/m^6A/BCAT1-2 axis reprograms BCAA metabolism in AML

BCAT1/2 transfer the amino groups from BCAAs to α-ketoglutarate to generate BCKAs and glutamate. In AML cells, *METTL16* KO resulted in significant upregulation of BCAAs, which could be completely reversed by restoration of METTL16 expression (Figures 7A and S7A). In addition, *METTL16* KO significantly decreased oxygen consumption rate (OCR), and again forced expression of METTL16 could restore the suppressed OCR in AML cells (Figures 7B-7D and S7B-S7D). Furthermore, we performed stable-isotope tracer (^{13}C,^{15}N-leucine) experiments coupled with liquid chromatography-mass spectrometry (LC-MS) to systemically delineate the role of METTL16 in reprogramming BCAA catabolism in AML cells (Figure 7E). Consistent with the decreased OCR, *METTL16* KO significantly attenuated the levels of metabolites belonging to the TCA cycle (Figures 7F and S7E). In addition, ^{15}N-leucine tracing analysis showed that *METTL16* KO significantly decreased the labeling of non-essential amino acids, such as Glu, Asp, Gly, Pro, Ser, and nucleotides (Figures 7G, 7H, S7F, and S7G). To further substantiate the role of METTL16 in BCAA metabolism, we cultured human AML cells upon *METTL16* KO in the medium with or without BCAA deprivation, and found that, compared to the parental AML cells, *METTL16* KO cells became more resistant to BCAA starvation (Figures 7I and S7H).

Finally, to determine whether BCAT1 and BCAT2 are required for the *METTL16* KO-mediated metabolism changes and cell survival/growth inhibition in AML, we performed rescue assays via overexpressing BCAT1 and BCAT2 in *METTL16* KO AML cells. As expected, forced expression of BCAT1 and BCAT2 could at least partially restore *METTL16* KO-induced AML cell proliferation defects and apoptosis (Figures 7J-7M, and S7I). More strikingly, ectopic expression of BCAT1 and BCAT2 could totally reverse *METTL16* KO-induced oxidative capacity inhibition (Figures 7N, 7O, S7J, and S7K), demonstrating that the effects of METTL16 expression manipulation on metabolism could be largely due to the dysregulation of BCAT1 and BCAT2. A previous study reported that METTL16 controls SAM biosynthesis by regulating the alternative splicing of SAM synthetase MAT2A.[31] To exclude the possibility that *METTL16* KO-induced leukemia metabolism reprogramming is attributed to SAM availability, we conducted additional rescue assay with SAM. As shown in Figures S7L-S7N, SAM treatment could not rescue *METTL16* KO-induced proliferation suppression and metabolism inhibition in AML cells. Collectively, our results indicate that *BCAT1* and *BCAT2* are functionally essential targets of METTL16 and contribute to METTL16's oncogenic role in AML.

DISCUSSION

In line with the CRISPR-Cas9 screening data that METTL16 shows much stronger dependency than METTL3 and METTL14 in AML cells, our *in vivo* functional studies

demonstrated that depletion of *METTL16* almost completely inhibited AML development/progression and at least doubled the overall survival in the BMT, xenotransplantation and PDX AML models, showing a stronger inhibitory effect than did depletion of *METTL3* or *METTL14*.[18,19,28] Strikingly, *METTL16* depletion resulted in 10-200-fold decrease of LSC/LIC frequency, highlighting the critical role of METTL16 in LSC/LIC self-renewal. Although homozygous KO of *Mettl16* showed moderate effects on normal hematopoiesis under steady conditions and a significantly inhibitory effect on normal HSC self-renewal/reconstitution under competitive stress conditions, heterozygous KO (i.e., haploinsufficiency) of *Mettl16* showed no significant effects on normal hematopoiesis or HSC self-renewal, which is opposite to the significantly inhibitory effect of *Mettl16* haploinsufficiency on leukemogenesis. Moreover, METTL16 is largely dispensable for the survival/proliferation/repopulation of human HSPCs. Thus, our results suggest that there is a good therapeutic window for targeting METTL16 to treat AML. We further showed that thousands of mRNA targets have decreased m^{6}A levels upon *METTL16* KO and hundreds of them with significantly changes in expression levels. We demonstrated that the catalytic activity of METTL16 is required for its oncogenic role in AML, because ectopic expression of loss-of-function mutations (PP185/186AA and F187G), unlike that of wildtype METTL16, couldn't reverse the phenotypes induced by *METTL16* KO at all. We also identified *BCAT1* and *BCAT2* as *bona fide* direct targets of METTL16 in AML and showed that METTL16 adds m^{6}A on their mRNA transcripts. METTL16 stabilizes their stability through YTHDC1, thereby promoting their expression in an m^{6}A- and YTHDC1-dependent manner, which in turn contributes to METTL16's oncogenic role in AML. Notably, opposite to the requirement of its catalytic activity for the oncogenic role of METTL16 in AML as shown herein, our previous study showed that METTL16 plays a critical oncogenic role in liver cancer through both catalytic activity-dependent (as an m^{6}A writer) and -independent (as a translation facilitator) mechanisms.[36] Thus, our studies suggest that the mechanisms underlying the pathological roles of METTL16 in different cancer types could be context-dependent, which warrants systematic investigation in the future. In addition, different from the previously identified targets of METTL16 (including U6 snRNA, *MALAT1*, *XIST*, and *MAT2A*) that contact a specific "duckbill"-like stem-loop motif (UACm^{6}AGAGAA),[31,34,35,37] neither *BCAT1* nor *BCAT2* mRNA contains such a motif; instead, they contain canonical "DRACH" m^{6}A motifs, suggesting that METTL16 targets diverse mRNAs with different motifs.[36]

Although the role of m^{6}A modification in tumor glycolysis and glutamine metabolism has been reported very recently,[22,55] its function in tumor amino acid metabolism remains elusive. Here we show for the first time that METTL16 and the associated m^{6}A modification play an essential role in regulating a critical tumor amino acid metabolism pathway, i.e., the BCAA metabolism pathway, by post-transcriptionally promoting expression of key enzymes (e.g., BCAT1 and BCAT2) in this pathway. Both the cytosolic BCAT1 and the mitochondrial BCAT2 are the enzymes that are responsible for the reversible transamination of BCAAs, including valine, leucine, and isoleucine. BCAT1/2 convert BCAAs into their corresponding BCKAs by transferring the amino group onto α-KG and thereby generating glutamate. The BCKAs are subsequently decarboxylated to form derivatives of coenzyme A (CoA), acetyl-CoA and succinyl-CoA, which are consumed in mitochondria, feed into

the TCA cycle, and contribute to energy production.[14,56] Furthermore, BCAAs can act as the sources of nitrogen for *de novo* nucleotide biosynthesis through the glutamate-glutamine axis. Therefore, BCAT1/2 reprogram the cancer metabolism as the multi-level regulators of TCA cycle, oxidative phosphorylation, and nucleotide biosynthesis to fuel the malignant and rapid expansion of tumor cells. More importantly, BCAA pathways as well as the BCAT1 expression levels are highly enriched in AML LSCs/LICs, and depletion of *BCAT1* leads to the accumulation of α-KG, accompanied with growth defect and LSC/LIC eradication in AML.[11] Such data is consistent with our discoveries that METTL16 is especially overexpressed in LSCs/LICs and *BCAT1* and *BCAT2* are two functionally essential targets of METTL16 in AML. Therefore, by post-transcriptionally regulating expression of *BCAT1* and *BCAT2* in an m^6A-dependent manner, METTL16 plays a critical oncogenic role in regulating BCAA metabolism and promoting LSC/LIC self-renewal.

In summary, our studies have revealed the strong dependency of METTL16 for the survival and stemness of AML cells. We have also uncovered a previous unappreciated signal pathway involving METTL16, m^6A modification, BCAT1 and BCAT2 in the pathogenesis of AML, leukemia metabolism, and LSC/LIC self-renewal. Since METTL16 likely plays a more critical oncogenic role than METTL3 and METTL14 in AML, suggesting that METTL16 represents a more attractive target for AML therapy. Moreover, different from our observation that KD of *METTL16* showed very mild inhibitory effects on the survival/proliferation of human $CD34^+$ HSPCs or mouse Lin^- HSPCs, KD of *METTL3* significantly and substantially inhibited survival/proliferation of human $CD34^+$ HSPCs,[19] suggesting that METTL3 is more essential than METTL16 for normal HSPC maintenance and proliferation. Notably, despite the fact that Mettl3 is very critical for embryonic development (Mettl3 KO is embryonic lethal) and normal hematopoiesis as well as normal HSC self-renewal, and METTL3 KD substantially suppresses human $CD34^+$ HSPC survival/proliferation,[19,57,58] pharmacological inhibition of METTL3 by a selective and potent inhibitor (STM2457) showed minor side effects on normal tissues (including blood system).[59] Thus, METTL16 should also be a safe target for AML therapy. Overall, METTL16 could be an even safer and more effective/promise therapeutic target than METTL3, given that compared to METTL3, METTL16 is much less required for human normal HSPC proliferation/repopulation but more essential for AML development and LSC/LIC self-renewal. Therefore, development of effective small-molecule inhibitors targeting METTL16 is of great translational/clinical significance and holds big potential for AML therapy.

LIMITATION OF THE STUDY

It is important to develop effective small-molecule inhibitors specifically targeting METTL16 and check whether such inhibitors can effectively kill AML cells (including LSCs/LICs) but spare normal HSPCs. Nevertheless, as constitutive homozygous KO of Mettl16 could cause embryonic lethal,[34] it is important to systematically check whether METTL16 inhibition is also safe for other types of normal tissues/cells besides the hematopoietic system. In addition, although our data suggest that METTL16 is likely a more effective/promise and safer therapeutic target than METTL3 for AML treatment, systematic studies are warranted to compare the therapeutic efficacy and safety between METTL16

inhibitors (when available) and METTL3 inhibitors in treating patients with AML or other types of cancers.

STAR METHODS

RESOURCE AVAILABILITY

Lead Contact—Further information and requests for reagents may be directed to and will be fulfilled by the Lead Contact, Xiaolan Deng (xideng@coh.org), or Jianjun Chen (jianchen@coh.org).

Materials Availability—All cell lines, plasmids, and other stable reagents generated in this manuscript are available from the Lead Contact under a complete Materials Transfer Agreement.

Data and Code Availability—The m^6A-seq and RNA-seq data generated in this study have been deposited in the gene expression omnibus (GEO) and made accessible under accession number GSE190045.

The m^6A-seq and RNA-seq data generated in this study have been deposited in the gene expression omnibus (GEO) and made accessible under accession number GSE190045.

This paper does not report original code.

Any additional information required to reanalyze the data reported in this work paper is available from the lead contact upon request.

EXPERIMENT MODEL AND SUBJECT DETAILS

Primary AML Patient and Healthy Donor Specimens—Human primary AML patient samples as well as the healthy donors were collected from bone marrow aspiration at the time of diagnosis, relapse, or remission after written informed consent at City of Hope Hospital, Cincinnati Children's Hospital, or Dana-Farber/Harvard Cancer Center in congruence with the protocol approved by the institutional review board (IRB). Characteristics of AML patients were outlined in Table S1. Leukemia blasts and mononuclear cells (MNCs) were isolated by Ficoll-Paque (17-1440-02, GE Healthcare Life Sciences) density centrifugation and cryopreserved at −150°C until used. Leukemia MNCs were cultured in IMDM medium (12440061, Thermo Fisher Scientific) supplemented with 20% fetal bovine serum (FBS) (10-437-028, Thermo Fisher Scientific), 1% Penicillin-Streptomycin (15-140-122, Thermo Fisher Scientific), 2.5 ug/ml Plasmocin prophylactic (ant-mpp, InvivoGen) and 10 ng/mL of rhSCF (250-03, PeproTech), rhTPO (300-18, PeproTech), rhFlt-3L (300-19, PeproTech), rhIL-3 (200-03, PeproTech), and rhIL-6(200-06, PeproTech). For transduction of primary patient samples, 6-well plates were coated with Retronectin (T202, Takara) at 4°C overnight or 2 hours at room temperature. Viral supernatant was added to Retronectin-coated plates and centrifuged for 2 hours at 2,000 g at 32°C. Primary AML patient cells were then seeded onto the plates followed by centrifugation for 30 min at 600 x g at 32°C. Infected cells were selected with 2ug/mL puromycin (ant-pr-1, InvivoGen) for 4 days to generate stable integration.

Isolation, Culture and Transduction of CD34+ HSPCs—The $CD34^+$ HSPCs cells were isolated from Umbilical Cord Blood (UCB) samples, which were purchased from StemCyte under the IRP protocol approved by City of Hope. Briefly, the MNCs were isolated from UCB by Ficoll-Paque density gradient centrifugation. $CD34^+$ cells were enriched from the mononuclear cells using Human CD34 MicroBead Kit (130-046-702, Miltenyi Biotec) and MACS Separator according to the manufacturer's protocols. Flow cytometry was performed after enrichment to assess the purity of $CD34^+$ cells. The $CD34^+$ HSPCs cells were cultured in SFEM medium supplemented with rhTPO (10 ng/mL), rhFlt-3L (10 ng/mL), rhIL-3 (10 ng/mL), rhIL-6 (10 ng/mL) and rhSCF (100 ng/mL).

Transduction of $CD34^+$ HSPCs cells was employed as described above for transduction of primary patient samples.

Cell Culture—All cell lines were obtained from the sources listed in the Key Resources Table. The leukemia cells, THP1, NB4, HL-60, NOMO-1, MOLM-13, HEL, ML-2 and Kasumi-1 were cultured in RPMI1640 (11875119, Thermo Fisher Scientific) supplemented with 10% FBS; OCI-AML3 was maintained in alpha-MEM (32571101, Thermo Fisher Scientific) supplemented with 10% FBS; MonoMac 6 (MMC6) was maintained in RPMI1640 supplemented with 10% FBS plus 2 mM L-glutamine (25030-081, Thermo Fisher Scientific), 1x non-essential amino acids (11140050, Gibco), 1 mM sodium pyruvate (11360070, Thermo Fisher Scientific) , 10 μg/ml human insulin (12585014, Thermo Fisher Scientific); KG-1a were maintained in IMDM supplemented with 10% FBS; MA9.3ITD (MLLAF9 plus FLT3-ITD-transformed human CD34+ cord blood), established by Dr. James Mulloy[67], were maintained in IMDM supplemented with 20% FBS. OP9 cells were cultured in Alpha-MEM supplemented with 20% plus 2.2 g/L sodium bicarbonate. HEK293T were maintained in DMEM supplemented with 10% FBS. All cells were routinely tested for mycoplasma contamination by a PCR Mycoplasma Detection Kit (G238, Applied Biological Materials Inc.). Penicillin-Streptomycin and Plasmocin prophylactic were supplemented in all media to prevent potential contamination. The identities of all cell lines were authenticated through short tandem repeat (STR) analysis.

Animals—All experiments on animals were performed in accordance with institutional guidelines and IACUC protocol approved by City of Hope. The “human-in-mouse” xeno-transplantation leukemia model used for *in vivo* bioluminescence imaging was established by transplanting 6-8 old NOD.Cg-Rag1^{tm1Mom} I12rg^{tm1Wjl} Tg (CMV-IL3, CSF2, KITLG) 1Eav/J (NRGS, RRID: IMSR JAX:024099) mice with AML cells. NRGS mice were obtained from Jackson laboratory and were maintained and bred under pathogen-free conditions. Both male and female NRGS mice were used for the experiments. 6-8 weeks old NCI B6-Ly5.1/Cr and NCI C57BL/6 female mice were purchased from Charles River Laboratories and use for allogeneic bone marrow transplantation. NCI C57BL/6 mice were used as donors. NCI B6-Ly5.1/Cr female mice were used as congenic recipients. Mouse model of MLL-AF9 were established by transplanting leukemic cells into NCI B6-Ly5.1/Cr. C57BL/6J (CD45.2) background Mettl16$^{fl/fl}$ mice were obtained from Cyagen. Mx1-cre mice were purchased from the Jackson Laboratory. Mett116$^{fl/fl}$ mice were generated by inserting floxed LoxP sites flanking exon 3. 6–8 weeks old C57BL/6J (CD45.2) using

CRISPR mediated strategy. Mettl16$^{fl/fl}$ mice were mated to Mx1-Cre transgenic mice to generate Mettl16$^{fl/+}$ Mx1Cre and Mettl16$^{fl/fl}$ Mx1Cre mice. Mx1-Cre expression could be induced by seven times of Polyinosinic: polycytidylic acid (poly(I:C)) i.p. injection every other day. The details of all experiments on animals involved are provided in the methods details section. All the mice were maintained on a 12hours: 12hours light-dark cycle with food and water ad libitum. Mice were randomly assigned into each group.

METHOD DETAILS

Analysis of Gene Dependency by DepMap—The CERES score for METTL family members were downloaded from the CRISPR (Avana) Public Depmap v20Q4 portal (https://depmap.org/portal/download/),. A gene with a lower CERES score indicates a higher likelihood that the gene is essential in a given cell line. A cell line is considered dependent if it has a probability of dependency greater than 0.5. A score of 0 indicates a gene that is not essential, while a score of −1 corresponds to the median of all common essential genes. For each METTL gene, the essentiality effect on leukemia cells was visualized using violin plots.

SgRNA Library Design and CRISPR Screen—Guide RNA sequences of DNA and RNA methylation focused CRISPR library (900 sgRNAs targeting 36 genes at 25 sgRNAs per gene) together with 22 sgRNAs targeting commonly essential genes (e.g., *MYC, BRD4, RPA3,* etc.) and 41 sgRNAs targeting non-essential sequences were designed using the Genetic Perturbation Platform (Broad Institute).[68] All the sgRNA sequence were outlined in Table S2. Briefly, sgRNA oligonucleotides were synthesized via microarray (CustomArray) and cloned into the ipUSEPR lentiviral sgRNA vector (hU6-driven sgRNA co-expressed with EF-1α-driven red fluorescent protein [RFP] and puromycin-resistance gene) using the BsmBI (NEB) restriction sites. All gRNA sequences were listed in Table S1. For CRISPR screening, Cas9-expressing single clones were infected with lentiviruses containing the sgRNA library at a multiplicity of infection (MOI) < 0.5. Two days after infection, cells were selected with 2μg/ml puromycin. Genomic DNA was extracted from each screen at day 0 and day 28. The integrated sgRNA-containing regions were amplified by PCR using primers DCF01 5'-CTTGTGGAAAGGACGAAACACCG-3' and DCR03 5'-CCTAGGAACAGCGGTTTAAAAAAGC-3'. Amplicon sequencing was performed on an Illumina NextSeq 500 sequencer. To quantify sgRNA reads, 20-nucleotide sequences that matched the sgRNA backbone structure (5′ prime CACCG and 3′ prime GTTT) were extracted from FASTQ files and aligned to the sgRNA sequences of the CRISPR screening library using Bowtie2. The frequency for individual sgRNAs was calculated as the read counts of each sgRNA divided by the total read counts matched to the library. For our CRISPR screening, the CRISPR score was defined as a log10-fold-change in the frequency of individual sgRNAs between the end (day 28) and starting time points (day 0) of the screened samples, calculated using the edgeR R package.

CRISPR/Cas9 Based Genome-Editing—For CRISPR/Cas9 based genome-editing, lentiCas9-Blast (52962, Addgene) and lenti-sgRNA hygro (104991, Addgene) vectors were used. The single Cas9 clones of NOMO-1, MMC6 and THP1 cells were constructed by infecting with lentiCas9-Blast lentiviruses and selecting with 10ug/mL blasticidin

(ant-b1-1, Invivogen). The lenti-sgRNA hygro vector was digested with BsmBl (R0739, NEB), purified with Gel Extraction Kit (28706X4, Qiagen) and used in the ligation reaction. All sgRNA sequences used in this manuscript were designed using CRISPick (https://portals.broadinstitute.org/gppx/crispick/public) and synthesized by Integrated DNA Technologies (IDT). The gRNAs were subsequently cloned into lenti-sgRNA hygro vector using DNA Ligation Kit (6023, Takara). All gRNA sequences targeted *METTL16* were listed in Table S1.

Plasmid Construction—The wild-type (pcDNA3-METTL16-WT) and mutant forms of METTL16 (pcDNA3-METTL16-PP185/186AA and pcDNA3-METTL16-F187G) plasmids were kindly provided by Dr. Nicholas K. Conrad. These plasmids were used as templates to generate wild-type METTL16 and mutant forms of METTL16 (METTL16-PP185/186AA and METTL16-F187G) fragments by PCR amplification with CloneAmp™ HiFi PCR Premix (639298, Takara Bio) using primers with XbaI (FD0684, Thermo Fisher Scientific) and NotI (FD0595, Thermo Fisher Scientific) restriction sites. The PCR fragments were ligated into pMIRNA1 to generate C-terminal 3 × FLAG-tagged WT-METTL16 and its corresponding mutant (pMIRNA1-METTL16-PP185/186AA and pMIRNA1-METTL16-F187G) with In-Fusion HD Cloning Plus Kits (638909, Takara Bio). The pMIRNA1-3×FLAG-METTL16-MUT1 and pMIRNA1-3×FLAG-METTL16-MUT2 were constructed based on 3 × FLAG-tagged WT-METTL16. The pMIRNA1-METTL16-PP185/186AA-MUT1, pMIRNA1-METTL16-F187G MUT1 were constructed based on pMIRNA1-METTL16-PP185/186AA and pMIRNA1-METTL16-F187G. The wild-type BCAT1 and BCAT2 were cloned by PCR amplification using cDNA as templates. BCAT1 fragments were ligated into pSIN4 to generate pSIN4-BCAT1, while BCAT2 fragments were ligated into pMIRNA1 to generate pMIRNA1-BCAT2. All of the In-fusion primers used in this study are listed in Table S3. All plasmids generated in this study were confirmed by sequencing (Eton Bioscience Inc.) and purified with QIAprep Spin Miniprep Kit (27106, Qiagen).

Lentivirus Preparation and Infection—Lentiviral particles for sgM16-1, sgM16-2, sgNS, pMIRNA1-3×FLAG-METTL16-MUT1, pMIRNA1-3XFLAG-METTL16-MUT2, pMIRNA1-METTL16-PP185/186AA-MUT1, pMIRNA1-METTL16-F187G MUT1, pMIRNA1, pLKO.1-shM16-1 (TRCN0000136815, Sigma-Aldrich), pLKO.1-shM16-2 (TRCN0000136881, Sigma-Aldrich), pLKO.1-shYTHDC1-1, pLKO.1-YTHDC1-2, pLKO.1-IGF2BP2-1, pLKO.1-IGF2BP2-2, pLKO.1-shNS, pSIN4-BCAT1, pSIN4, pCDH-1xFLAG-BCAT2 and pCDH were packaged in HEK-293T cells. Lentiviral particles were generated by co-transfecting cells with 2 ug lentiviral vector containing sequences of interest, 0.75 ug pMD2.G (12259, Addgene), and 2.25 ug psPAX2 (12260, Addgene) using X-tremeGENE™ HP DNA Transfection Reagent (Sigma-Aldrich, 6366236001) in 60mm cell-culture dishes (Bioland Scientific). After 24hr, the transfection medium (Opti-MEM™ I Reduced Serum Medium, 31985070, ThermoFisher) may be replaced with complete DMEM medium. Virus-containing supernatant was collected 48h and 72h post transfection and centrifuged for 30min at 3000g at 4°C. For infecting leukemia cells, viral supernatant was added to cells in the presence of 4 ug/mL polybrene (H9268, Sigma-Aldrich). Two rounds of spinoculation at 1200rpm, 32°C for 2h were carried out to increase

transduction efficiency. The infected cells were subjected to hygromycin B (ant-hg-1, Invivogen) selection (for sgM16-1, sgM16-2 and sgNS) at 1mg/mL or puromycin selection (for pLKO.1-shM16-1, pLKO.1-shM16-2, pLKO.1-shYTHDC1-1, pLKO.1-YTHDC1-2, pLKO.1-IGF2BP2-1, pLKO.1-IGF2BP2-2 and pLKO.1-shNS) at 2ug/mL for additional 96h.

Protein Extraction and Immunoblot Analysis—Cells were harvested by centrifugation at 800rpm for 5min, washed with cold PBS and lysed in RIPA buffer (R0278, Sigma-Aldrich) supplemented with 1% protease inhibitor cocktail (78438, Thermo Fisher Scientific) and phosphatase inhibitor cocktail (78426, Thermo Fisher Scientific). The samples were incubated on ice for 30 min and sonicated to fragment chromatin. Cell lysate was centrifuged at 20,000 x g for 15 min at 4°C, and supernatants were collected. Protein concentration was measured using Bio-Rad Protein Assay Dye Reagent Concentrate (5000006, Bio-Rad) with bovine serum albumin (Protein Standard II #5000007, Bio-Rad) as a protein standard. Protein lysates were diluted with 4× Laemmli Sample Buffer (5000007, Bio-Rad) containing 2-mercaptoethanol and denatured at 99°C for 10min.

Immunoblot analysis were conducted as previously described.[20,43] Briefly, equal amounts of protein extracts (20-50ug) were loaded on 10% SDS-PAGE gels and transferred to PVDF membranes for further immunoblot analysis. The blots were incubated with primary antibodies in 1% (w/v) BSA in PBST overnight at 4°C. After incubation, membranes were washed with PBST, and then incubated with secondary antibody for 1h at room temperature. Primary antibodies used in this study include anti-METTL16 (1:1000, HPA020352, Millipore Sigma), anti-METTL16 (1:3000, A304-192A, Bethyl), anti-Vinculin (1:5000, sc-25336, Santa Cruz Biotechnology), anti-BCAT1 (1:1000, TA504360S, OriGene Technologies), anti-BCAT2 (1:1000, 16417-1-AP, Proteintech), anti-LARS1 (1:1000, 21146-1-AP, Proteintech), anti-β-Actin (1:5000, 3700, Cell Signaling Technology). Secondary antibodies used in this study include Goat Anti-Mouse IgG H&L (HRP) (ab6789, abcam) and Goat Anti-Rabbit IgG H&L (HRP) (ab6721, abcam).

Cell Proliferation Assay—Cell proliferation was assessed using CellTiter 96® Non-Radioactive Cell Proliferation Assay (MTT, G400, Promega). Cells were transduced with lentivirus by spinoculation and selected with corresponding antibiotics for 4 days to generate stable cells. After selection, the cells were seeded into 96-well plates at a concentration of 8, 000-10, 000 cells per in triplicate in a final volume of 100 μl. Following the manufacturer's recommendation, 15 μl dye solution was added to each well every 24h for 6 consecutive days. After incubation at 37°C for 2-4h, 100ul solubilization/stop solution was added to quench the reaction. Finally, the absorbance at 570 nm was determined using a microplate reader on the next day.

Cell Differentiation and Apoptosis Analysis with Flow cytometry—To evaluate cell differentiation status, cells were harvested, washed with ice-cold PBS and resuspended in Flow Cytometry staining buffer (00-4222-26, eBioscience). The cells were stained with following antibodies on ice for 30min: PE-CD11b (101207, Biolegend), APC-CD14 (17-0149-42, eBioscience), APC-CD11b (50-112-3031, eBioscience), PE-Gr1 (12-5931-81, eBioscience). After incubation, cells were washed with staining buffer and then subjected to flow cytometry analysis.

To assess cell apoptosis, cells were performed 7-AAD and Annexin V staining with Annexin V Apoptosis Detection Kit (88-8007-74, eBioscience) according to the manufacturer's instructions. The cells were subjected to flow cytometry and analyzed with FlowJo.

Retrovirus Preparation, Colony Formation, and Serial Plating Assay—These assays were performed as described previously with minor modifications.[69,70] Briefly, retroviruses particles were generated by co-transfecting HEK-293T cells with 1.2ug pCL-Eco packaging vector (IMGENEX, San Diego, CA) and 1.6ug individual retroviral construct. Virus-containing supernatant was collected 48h and 72h post transfection and centrifuged for 30min at 3000g at 4°C. To isolate the lineage-negative (Lin-) HSPCs from bone marrow, the 4- to 6-week-old B6.SJL (CD45.1) female mice were administrated with 5-fluorouracil (5-FU) (150 mg/kg) for five days. Then, the Lin- cells were enriched with BMMNCs Lineage Cell Depletion Kit (130-090-858, Miltenyi Biotec) and infected with MSCVneo-based and/or MSCV-PIG-based retroviruses and shRNA lentiviruses in the presence of 4 ug/mL polybrene through two rounds of "spinoculation" *at 1800rpm* 32°C for 2h. The transduced cells were seed at a density of 1 x 10^4 per 35 mm culture dishes (27150, STEMCELL Technologies) in Methylcellulose-based Media (ColonyGEL™ 1201, ReachBio Research Labs) supplemented with 10 ng/ml of murine recombinant IL-3, IL-6, GM-CSF and 50 ng/ml of murine recombinant SCF, along with 1.0 mg/ml of G418 (GIBCO BRL, Gaithersburg, MD) and/or 2ug/mL of puromycin. The colonies were counted after 6-7 days of incubation at 37°*C.* For the serial replating assay, the colonies were harvested, and *1* × 10^4 cells were subsequently replated in fresh Methylcellulose-based Media. Three rounds of replating were conducted.

For CFA assays of $CD34^+$ blast cells derived from human primary samples, the cells were transduced with lentivirus and then seeded into MethoCult H4434 Classic medium (StemCell Technologies) supplemented with 2 μg/ml puromycin. The colonies were counted after 10 days of incubation at 37°C.

Murine Bone Marrow Transplantation (BMT)—For primary BMT assay, bone marrow cells were isolated from 4- to 6-week-old C57BL/6J (CD45.2) female mice treated with 5-FU, and Lin- cells were enriched following the aforementioned strategies. Subsequently, the Lin- cells were infected with MSCV-Neo-MA9 retroviruses in the presence of 4 ug/mL polybrene through two rounds of "spinoculation" at 1800rpm 32°C for 2h. After 7 days of selection with 1.0 mg/ml of G418, the infected cells (3×10^5) plus 1×10^6 "helper" cells (bone marrow mononuclear cells extracted from B6.SJL (CD45.1) female mice were transplanted into lethally irradiated (900 rads) 8 to 10 weeks old B6.SJL (CD45.1) female recipient mice. Recipient mice transplanted with Mettl16 Mx1-cre cells were injected with poly (I:C) intraperitoneally 7 days after transplantation. For secondary BMT assay, leukemia cells sorted from bone marrow of primary leukemia mice were injected into sub-lethally irradiated (450 rads) recipient mice.

Leukemia Engraftment Analysis—Peripheral blood, bone marrow samples and spleen samples were collected from recipient mice at the same time point for each group. The cells were re-suspended in Ammonium Chloride Solution (07850, STEMCELL Technologies) to deplete red cell, washed with PBS, re-suspended in FACS buffer and stained with APC-

CD45.2 (17-0454-82, eBioscience) at 4°C for 30min. After staining, the cells were washed with FACS buffer and subjected to flow cytometry analysis.

Histopathology Analysis—The recipient mice in control group were euthanized by CO_2 inhalation when they showed signs of systemic illness, and the recipient mice in other groups were also sacrificed at same time to collect specimens for histopathology analysis. PB and BM cells were smeared on slides and performed Wright-Giemsa staining. Portions of the spleen and liver were employed to paraffin embedding and H&E staining. All the slides were captured by a Widefield Zeiss Observer 7 microscope.

Limiting Dilution Assay—For *in vivo* limiting dilution assay, 1×10^6, 1×10^5, 1×10^4, 1×10^3, 1×10^2 bone marrow mononuclear cells (BMMNCs) were collected from primary BMT mice (3 mice/group), which were euthanized at the same time, and then were mixed and transplanted into sub-lethally irradiated 8 to 10 weeks wild-type B6.SJL (CD45.1) female recipient mice through tail vein. The mice were monitored for leukemogenesis for 8 weeks. For *in vitro* limiting dilution assay, the murine MA9 AML cells with or without *METTL16* depletion were seeded at a density of 100, 50, 20, 10, 5 per 35 mm culture dish in Methylcellulose-based Media. The colonies were cultured for 2 weeks. The frequency of leukemia stem/initiating cells (LSCs/LICs) were determined by ELDA software (http://bioinf.wehi.edu.au/software/elda/).

Surface and Intracellular Staining—Human primary AML cells were washed with ice-cold PBS and stained with anti-CD34 FITC for 30min at 4°C. The cells were then washed with ice-cold PBS, fixed in 4%-paraformaldehyde (158127, Sigma-Aldrich) and incubated at 4°C for 20min with rotation. The fixed cells were re-suspended in 5 x Permeabilization buffer (00-8333-56, eBioscience) and incubated at 4°C for 30min. The cells were re-suspended in 1 x Permeabilization buffer and stained with rabbit anti-human METTL16 (1:100) for 1h at 4°C, mixed every 10min. Finally, the cells were stained with goat anti-rabbit IgG (H+L) (Alexa Fluor 555 Conjugate, 4413S, Cell Signaling Technology) for 30min at room temperature, washed twice with1 x Permeabilization buffer and re-suspended in FACS buffer for further analysis. For mice cells, bone marrow cells were extracted from 4 to 6 weeks old B6.SJL (CD45.1) female mice. The BM cells were stained with anti- lineage markers and rabbit anti-mouse Mettl16 (1:100) as described for human cells.

Xenotransplantation Experiments—Both female and male NRGS mice were used as hosts for xenotransplantation experiments. For each experiment, both female and male mice were randomly assigned into each group. MA9.3ITD and $Cas9^+$ MMC6 cells were transduced with pLenti CMV Puro LUC (17477, Addgene) lentiviruses and selected with 2ug/mL puromycin for 4 days. Then MA9.3ITD and $Cas9^+$ MMC6 cells were infected with indicated construct. 1 x 10^5 CTL, METTL16 KO, METTL16 KO rescued with WT METTL16 MMC6 or 1 x 10^5 shNS/shM16 MA9.3ITD cells were re-suspended in PBS and transplanted into 8-10 weeks NRGS recipient mice intravenously. To monitor AML progression, *in vivo* bioluminescence imaging was conducted on the recipient mice weekly. To assess AML burden, mice were euthanized at the same time and stained with anti-human

BV786-cojugated anti-CD45 (563716, BD Bioscience). After staining, cells were subjected to flow cytometry.

In addition, we used three AML patient samples, including #2017-129, HTB22-0148 and #2016-25, to construct PDX mouse model. For #2017-129 1st BMT, we have transplanted 1.75×10^5 primary cells (non-passaged) into busulfan-conditioned NSGS mice via intrafemoral injection and the recipient mice will develop AML within 100 days. Then, the AML cells were isolated from spleens of 1st recipients and used for 2nd BMT (1×106 cells/NSGS), and the 2nd recipients developed AML within 30 days. In our study, we have maintained the AML cells from spleens of 1st recipients in vitro for lentivirus transduction to mediate METTL16 KO and implanted 1×10^6 cells into the NRGS mice. For HTB22-0148, we transduced primary AML cells with lentivirus to mediate METTL16 KO, and immediately transplanted these cells into NRGS mice (5×10^6 cells/recipient; tail vein injection). Regarding #2016-25, we first transplanted 2.5×10^6 primary cells (non-passaged) into busulfan-conditioned NRGS mice via tail vein injection and the recipient mice will develop AML within 42 days. Then, the AML cells were isolated from spleens of 1st recipients, and we maintained these AML cells in vitro for lentivirus transduction. Afterward, we implanted 5×10^6 cells into the NRGS mice. To assess AML burden, mice were euthanized at the same time and stained with anti-human PE-cojugated anti-CD33 (12-0339-42, Thermo Fisher Scientific). After staining, cells were subjected to flow cytometry.

In vivo* Bioluminescence Imaging—In vivo* bioluminescence imaging assay was used to monitor *in vivo* engraftment of MA9.3ITD and MMC6 cells in NRGS recipient mice. D-luciferin (LUCK-2G, Goldbio) was dissolved in PBS. For *in vivo* bioluminescence imaging, mice were weighed, injected with 150mg/kg D-luciferin and then anesthetized using isoflurane. Whole-body bioluminescence imaging was performed with Lago X (Spectral Instruments Imaging) at 10min after D-luciferin injection. The bioluminescence signal was presented in radiance in a unit of "photons/seconds/cm^2/steradian". The pseudocolor indicates the signal strength for leukemia burden.

Leukemia Stem Cell Analysis—For leukemia stem cell analysis, bone marrow cells were collected from primary BMT recipient mice and resuspended in ammonium chloride solution to lysate red cells. After washing, cells were stained at 4°C with various antibodies diluted in Flow Cytometry Staining Buffer (eBioscience) for 30 minutes. After incubation, cells were resuspended in IC Fixation Buffer (eBioscience) before being loaded for flow cytometry analysis in BD FACS FortessaX-20. The following antibodies were used for flow cytometry: anti-CD45.2-FITC (109806, BioLegend), anti-lineage markers-eFluor™ 450 (88-7772-72, eBioscience), c-Kit-APC (17-1171-82, eBioscience), Sca-1-PE (12-5981-82, eBioscience), CD16/CD32-APC/Cyanine7 (156612, BioLegend), and CD34-PE/Cyanine7 (119326, BioLegend).

Isolation of HSC and Lineage Cells from Murine BM—Bone marrow cells were extracted from 4 to 6 weeks old B6.SJL (CD45.1) female mice and resuspended in ammonium chloride solution to lysate red cells. After counting, lineage cells were enriched with specific microbeads according to the manufacturer's instructions. Briefly, Lin^- and

Lin^+ cells were separated with the Lineage Cell Depletion Kit, whereas $Mac1^+$ and $Gr1^+$ cells were purified by staining cells with CD11b-Biotin (clone M1/70.15.11.5, 130-098-582, Miltenyi Biotec), Gr-1-Biotin (clone RB6-8C5, 130-101-894, Miltenyi Biotec) antibodies, respectively, follow by incubating with Anti-Biotin MicroBeads UltraPure (130-105-637, Miltenyi Biotec) and then applying to MACS seperation columns (Miltenyi Biotec).

OP9 Co-culture Assay—Coculture of mouse HSPCs with OP9 cells were performed as described previously[28] with some modifications. Briefly, 3×10^5 OP9 cells were pre-seeded onto 6 well plate in α-MEM medium containing 2.2 g/L sodium bicarbonate, 20% FBS, 100 U/mL Penicillin/Streptomycin, and grown to 80-90% confluence. Lin^- HSPCs were enriched from bone marrow mononuclear cells of wild-type B6.SJL (CD45.1) mice and $0.1x10^6$ cells were seeded in 2 mL OP9 medium onto the OP9 cells with the addition of 10 ng/mL of mouse IL-3, human IL-6, mouse IL-7, Flt-3L, and 50 ng/mL mouse SCF. At day 3 and day 5, cells were disaggregated without the use of trypsin and filtered through a 40 μm cell strainer, and collected for analysis by immunoblot, qPCR or flow cytometry.

Phenotypic Analysis of Hematopoiesis—Phenotypic analysis of hematopoiesis was performed as previously described[71,72] with some modifications. Both male and female $Mettl16^{fl/fl}$;Mx1-Cre mice were used for the experiments. Briefly, peripheral blood was collected from tail vein and were performed on an element HT5 (HESKA) according to the manufacturer's protocol. HSPC populations in mouse bone marrow were analyzed, including HSC ($Lin^-Sca\text{-}1^+$ $c\text{-}Kit^+$ $CD48^-$ $CD150^+$); MPP ($Lin^-Sca\text{-}1^+$ $c\text{-}Kit^+$ $CD48^-$ $CD150^-$); HPC1 (Lin^- $Sca\text{-}1^+$ $c\text{-}Kit^+$ $CD48^+$ $CD150^-$); HPC2 (Lin^- $Sca\text{-}1^+$ $c\text{-}Kit^+$ $CD48^+$ $CD150^+$); CMP (Lin- $Sca\text{-}1^-$ $c\text{-}Kit^+$ $CD16/32^{int}$ $CD34^{+/low}$); GMP (Lin^- $Sca\text{-}1^-$ $c\text{-}Kit^+$ $CD16/32^+$ $CD34^+$); MEP (Lin^- $Sca\text{-}1^-$ $c\text{-}Kit^+CD16/32^-$ $CD34^-$). For HSPC populations analysis, BM cells were lysed with ACK LYSING Buffer (VWR) to remove red blood cells, then incubated with antibodies in FACS buffer on ice for 30 minutes at dark and mix every 10 minutes. Mature cells populations in bone marrow and spleen were analyzed, including CD3-T cells, B220-B cells and Ter119-erythroid cells. For mature cells populations analysis, suspended single cells isolated from bone marrow and spleen were incubated with antibodies in FACS buffer on ice for 30 minutes at dark and mix every 10 minutes. After incubation, cells were resuspended in IC Fixation Buffer (eBioscience) before being loaded for flow cytometry analysis in BD FACS FortessaX-20.

The following antibodies were used for flow cytometry: anti-lineage markers-eFluor™ 450 (88-7772-72, eBioscience), c-Kit-APC (17-1171-83, eBioscience), Sca-1-PE (12-5981-82, eBioscience), CD150-PerCP-eFluor™ 710 (46-1502-82, Thermo Scientific), CD48-FITC (11-0481-82, eBioscience), CD16/CD32-APC/Cyanine7 (156612, eBioscience), CD34-PE/Cyanine7 (119326, BioLegend), CD3-APC (100236, BioLegend), B220-APC/Cyanine7 (BDB561102, BD Bioscience), Ter119-V450 (BDB560504, BD Bioscience), CD11b-PerCP-Cyanine5.5 (Mac1, 45-0112-82, eBioscience) and Gr1-PE (12-5931-81, eBioscience).

Competitive Repopulation Assay—BM cells (1×10^6, CD45.2) from 7~8 weeks Mettl16 WT, heterozygous KO (*Mettl16*$^{fl/wt}$*; Mx1*-Cre), and homozygous KO (*Mettl16*$^{fl/fl}$*;*

Mx1-Cre) female mice plus equal number of competitor BM cells (1×10^6, CD45.1) from 7~8 weeks B6.SJL female mice were transplanted into lethally irradiated (900cGy) B6.SJL(CD45.1) female mice by tail vein injection. Mice were injected with poly (I:C) intraperitoneally 7 days after transplantation. PB was collected by tail vein bleeding of the recipient mice and subjected to flow cytometric analysis with PE-CD45.1 and APC-CD45.2 antibodies every four weeks.

RNA Extraction and Quantitative RT-PCR Analysis—Total RNA was extracted from cells using TRIzol reagent according to the manufacturer's instructions. Reverse transcriptase reaction was performed with 200-1000 ng of total RNA or immunoprecipitated RNA samples using the QuantiTect Reverse Transcription kit (205314, QIAGEN) following the manufacturer's instructions. Quantitative real-time PCR (qPCR) was performed with Maxima SYBR Green qPCR Master Mix (2 X) (FEPK0253, Thermo Fisher) using a QuantStudio (TM) 7Flex Real-Time PCR system (Applied Biosystem). Target gene expression levels were normalized by house-keeping gene β-actin. All the primers used in qPCR analysis are listed in Table S3.

***In Vitro* Transcription—**All transcripts used in this study were synthesized using the MEGAscript™ T7 kit (AM1333, Invitrogen) and PCR DNA as a template according to the manufacturer's instructions. Briefly, the cDNAs were synthesized with total RNA extracted from MMC6 cells using Superscript™ III First-Strand Synthesis System (18080051, Invitrogen). Then, DNA templates including T7 promoter were PCR-amplified from cDNAs with specific primers fused to an upstream T7 promoter sequence using Platinum™ SuperFi II DNA Polymerase (12361010, Thermo Scientific). Primers employed to generate DNA templates are listed in Table S3. Transcription was performed using the MEGAscript™ T7 kit. DNA template was digested by TURBO DNase. Transcripts were purified by MEGAclear™ Transcription Clean-Up Kit (AM1908, Thermo Fisher Scientific).

***In Vitro* m^{6}A RNA Methylation Assay—**The single strand RNAs (ssRNAs) used in this study were synthesized by *in vitro* transcription using MEGAscript™ T7 kit. Prior to *in vitro* m^{6}A RNA methylation, the ssRNAs were refolded in 10 mM NaCl by heating in a thermoblock at 70°C for 5 min, and slowly cooling down to room temperature. All methylation reactions were performed in a 50 μl reaction mixture contained final concentration of 50 mM Tris-HCl (pH 7.5), 100 mM KCl, 5 mM $MgCl_2$, 1μM SAM, 20U RNase inhibitor (EO0382, Thermo Fisher Scientific), 2 mM DTT (43816, Sigma-Aldrich) with 2 μM of refolded ssRNAs, 5 μg of recombinant protein. The reactions were performed overnight at 37°C. The ssRNAs were purified by RNA Clean & Concentrator-5. Methylation was assessed by UHPLC-QQQ-MS/MS of digested nucleotides. The co-immunoprecipitated RNA were recovery by RNA Clean & Concentrator-5.

UHPLC-QQQ-MS/MS for Determination of m^{6}A/A Ratio—The levels of N6-methyladenosine (m^{6}A) and adenosine (A) were measured by ultra-high-performance liquid chromatography coupled with triple-quadrupole tandem mass spectrometry (UHPLC-QQQ-MS/MS). Purified RNA and mRNA were digested with 2U nuclease P1(N8630 Sigma) at 42°C for 2 h in 20 μl of buffer containing 20 mM NH4OAc, followed by the addition of

alkaline phosphatase (1U) (EF0651, Thermo Fisher Scientific) for 2 h at 37°C. The digestion mixture was diluted to 200 μl by LC-MS grade water containing 0.2 fmol/μL of m^6A-d3 as an internal standard. The digestion mixture was then filtered with PierceTM Protein Concentrator PES (MWCO, 3K, 0.5 mL, 88512, Thermo Fisher Scientific) and 10 μl of this solution was injected into the LC-MS/MS system. A, m6A were later separated by UPLC-ESI-QQQ on a C18 column (00A-4475-AN, Phenomenex). 0.1% formic acid (FA) in ddH2O as Solvent A and 0.1% FA in acetonitrile as Solvent B were employed as the mobile phase. The quantification was carried out using a standard curve generated from A, m^6A standards.

Gene-specific m^6A qPCR—To determine m^6A modification in a specific transcript, the gene-specific m^6A qPCR was performed accordingly.[20,28,43,71] Briefly, mRNA was purified from total RNA by PolyATtract mRNA Isolation Systems. 2ug mRNA was fragmented into 100~200 nt in length with RNA Fragmentation Buffer and one tenth of fragmented RNA was saved as input control. Then fragmented RNA was incubated with anti-m^6A antibody conjugated beads with rotation for 2h at 4°C. After washing 3 times with 1 × IP buffer, the m^6A IP portion were eluted twice with m^6A elution buffer. The eluates were purified by RNA Clean & Concentrator-5. Input RNA and MeRIP-ed RNA were further analyzed by qPCR using primers listed in Table S3. The related enrichment of m^6A in each sample was calculated by normalizing Ct values of the sample immunoprecipitated with anti-m^6A to the Ct values of the corresponding input portion.

RIP-qPCR—The RIP experiment was performed according to the protocol from Abcam (https://www.abcam.com/epigenetics/rna-immunoprecipitation-rip-protocol), with some modifications. Briefly, $CD34^+$ HSPCs, NOMO-1 and MMC6 cells with forced expression of 3 × FLAG-tag fused METTL16 were collected, washed with ice-cold PBS, lysed with 1ml M-PER Mammalian Protein Extraction buffer (78501, Thermo Fisher Scientific) with 1 × protease inhibitor, 1 × Phosphatase Inhibitor and 100 U/mL RNase inhibitor on ice for 30min and sonicated using a Bioruptor Pico at 4°C with 30s ON, 30s OFF for 10 cycles. After sonication, the lysate was centrifuged at 13,000rpm, 4°C for 15min. Then, supernatants were collected and incubated with FLAG antibody or Mouse-IgG antibody with rotation at 4°C overnight. The mixture was added to washed Protein A/G beads and rotated at 4°C for an additional 2 hr. The beads were washed with RIP buffer (150 mM KCl, 25 mM Tris (pH 7.4), 5 mM EDTA, 0.5 mM DTT, 0.5% NP40, 100 U/mL RNase inhibitor) for 3 times and re-suspended in PBS, followed by DNA digestion with DNase I (EN0521, Thermo Fisher Scientific) at 37°C for 30min and protein digestion with Proteinase K (EO0492, Thermo Fisher Scientific) for 55 °C for 1h. The co-immunoprecipitated RNA were recovered by RNA Clean & Concentrator-5 and analyzed by qPCR using primers listed in Table S3.

RNA Stability Assay—The cells upon *METTL16* depletion were treated with Actinomycin D (A9415, Sigma-Aldrich) for indicated time and harvested. Total RNA was extracted from cells using TRIzol reagent for reverse transcription and qPCR analysis. The half time of mRNA were estimated according to previously describe.[20,43] Since mRNA transcription was inhibited with Actinomycin D, the rate of degradation of mRNA

concentration at a given time (*dC/dt*) is proportional to both the constant of mRNA decay (k_{decay}) and mRNA concentration © as shown in the following equation:

$$dC / dt = -k_{decay}C$$

Thus, the mRNA degradation rate k_{decay} was estimated by the derivation of the equation:

$$\ln(C / C_0) = -k_{decay}t$$

C_0 is the concentration of mRNA at time 0, t is the transcription inhibition time, and C is the mRNA concentration at the time t. To calculate half-time ($t_{1/2}$), which means that 50% of mRNA was decayed (C/C0=50%/100%=1/2), the equation can be rearranged into the following equation:

$$\ln(1 / 2) = -k_{decay}t_{1/2}$$

from where:

$$t_{1/2} = ln2 / k_{decay}$$

Measurements of OCR Using the XFe96 Extracellular Flux Analyzer— Mitochondrial OCR was measured by Seahorse XFe96 Analyzer with Seahorse XF Cell Mito Stress Test Kit (103015-100, Agilent Technologies) according to the manufacturer's instructions. In brief, 0.5-1 × 10^5 cells per well were seeded in 96-well Seahorse plates with XF RPMI medium supplemented with 2 mM glutamine, 10 mM glucose, 1mM pyruvate, and 5 mM HEPES, and incubated in a CO_2-free incubator for 30 min prior to the assay. For assessment of mitochondrial respiratory activity, Oligomycin, FCCP and Rotenone/Antimycin A were injected through port A, B and C at 1.5 μM, 0.5–1 μM, and 1 μM (final concentration), respectively, according to the manufacturer's instructions. All data were normalized to cell number.

Quantification of BCAA Concentration—BCAA concentration *in cellulo* was determined using Branched Chain Amino Acid Kit (MAK003, Sigma-Aldrich) according to the manufacturer's instructions. NOMO-1 and MMC6 cells with or without METTL16 were collected, homogenized in cold BCAA Assay buffer, and centrifuged at 13,000 × g for 10 minutes at 4 °C to remove insoluble material. BCAAs were quantified in 100 μl (total volume) reaction mixture. The absorbance at 570 nm was determined using a microplate reader to calculate the concentration of BCAAs. Protein concentration was determined for normalization.

Leucine Tracing—For stable-isotope tracing experiments, the cells were plated into 6-well plates at 1 × 10^6 cells/well in 2 ml of pre-warmed RPMI (SKU:091629149, Mp Biomedicals) containing $^{13}C_6$, $^{15}N_1$-Leucine (CCN1600P01, CortecNet) instead of the regular Leucine and cultured for 24 hours. Then the cells were collected, rinsed with

ice-cold 5% mannitol, and quenched with 1 ml 80% methanol (−80 °C). The extracts were vortexed vigorously for 15s three times over a period of 30min while kept on ice, and then centrifuged at 16,000g for 5 min at 4 °C. The cleared supernatant was transferred to a new Eppendorf tube and evaporated under vacuum at 30°C using a Vacufuge plus - Centrifuge Concentrator (Eppendorf). Dried metabolite extracts were stored at −80°C. The mass spectrometry-based analysis of extracted metabolites was conducted at UCLA Metabolomics Center.

Metabolomics Analysis—Dried metabolites were resuspended in 50% ACN:water and 1/10th was loaded onto a Luna 3um NH2 100A (150 × 2.0 mm) column (Phenomenex). The chromatographic separation was performed on a Vanquish Flex (Thermo Scientific) with mobile phases A (5 mM NH4AcO pH 9.9) and B (ACN) and a flow rate of 200 µl/min. A linear gradient from 15% A to 95% A over 18 min was followed by 7 min isocratic flow at 95% A and reequilibration to 15% A. Metabolites were detection with a Thermo Scientific Q Exactive mass spectrometer run with polarity switching (+3.5 kV/− 3.5 kV) in full scan mode with an m/z range of 70-975 and 140.000 resolution. Maven v8.1.27.11) was used to quantify the targeted metabolites by area under the curve using expected retention time (as determined with pure standards) and accurate mass measurements (< 5 ppm). Values were normalized to cell number.

Relative amounts of metabolites were calculated by summing up the values for all measured isotopologues of the targeted metabolites. Metabolite Isotopologue Distributions were corrected for natural C13 abundance.[73,74]

Data analysis was performed using in-house R scripts.

RNA-seq and Data Analysis—For RNA-seq, total RNA extraction from CTL, METTL16 KO and METTL16 KO rescued with WT METTL16 NOMO-1 cells was performed using TRIzol reagent (15596-018, Thermo Fisher Scientific) according to the manufacturer's instructions. Total RNA was subjected to depletion of rRNA and assessment of RNA integrity by 2100 Bioanalyzer (Agilent Technologies, Santa Clara, USA). RNA library preparation was conducted using KAPA Stranded mRNA-Seq Kit (Illumina Platforms) (Kapa Biosystems, Wilmington, USA) with 10 cycles of PCR amplification and purified by AxyPrep Mag PCR Clean-up kit (Thermo Fisher Scientific). Libraries were run on an Illumina HiSeq 2500 (Illumina, San Diego, CA, USA) instrument in a 51 bp single-end run, generated by the TruSeq SR Cluster Kit V4-cBot-HS (Illumina). Sequencing reads were trimmed and aligned to human reference genome (version GRCh38) by STAR.[66] Per million mapped reads (RPKM) of each gene were calculated by RSEM.[65] Differential expression analysis between two different conditions was conducted in R using the Bioconductor package DESeq2. Gene Set Enrichment Analysis (GSEA) with differentially expressed genes was performed to identify enriched pathway. Differentially expressed genes between CTL, METTL16 KO, METTL16 KO rescued with WT METTL16 NOMO-1 cells were identified using a double threshold on gene expression changes and associated statistical significances (absolute log1.5 fold change > 0.5, P<005).

Methylated RNA immunoprecipitation sequencing (MeRIP-seq) and Data Analysis—For m6A-seq, total RNA was extracted from CTL, METTL16 KO NOMO-1 cells using TRIzol reagent. mRNA was further purified by PolyATtract® mRNA Isolation Systems (Z5310, Promega). 2ug mRNA was fragmented into 100~200 nt with RNA Fragmentation Buffer at 70°C for 10min. Then EDTA was added to quench the fragmentation reaction. Fragmented RNA was purified by RNA Clean & Concentrator-5 (R1014, Zymo Research). For immunoprecipitation, 5ug anti-m^{6}A antibody (202003, Synaptic Systems) was conjugated to Protein A/G magnetic beads by rotation for 30min at room temperature. Fragmented RNA was incubated with anti-m^{6}A antibody conjugated beads with rotation for 2h at 4°C. After incubation, the beads were separated, washed 3 times with 1 X IP buffer and then eluted twice with m6A elution buffer. The eluates were purified by RNA Clean & Concentrator-5. Both input and m^{6}A IP samples were subjected to library preparation with the TruSeq Stranded mRNA Library Prep Kit (Illumina, San Diego, CA) and sequenced on an Illumina Hiseq 2500. Reads from mRNA input and m6A IP sequencing libraries were aligned to human reference genome (version GRCh38) by STAR. The m^{6}A-enriched regions (peaks) were identified by exomePeak with default parameters.

QUANTIFICATION AND STATISTICAL ANALYSIS

Data were analyzed with GrapPad Prism 8 and were presented as mean ± SD as indicated. Statistical Significance was calculated using two-tailed, unpaired Student's t tests, paired t test, one-way ANOVA or two-way ANOVA. Statistical significance for survival was calculated by the log-rank test. Detailed information about the statistical methods used is specified in the figure legends or Methods. $P < 0.05$ was considered significant. All Western blotting images are representative of at least two independent experiments.

Supplementary Material

Refer to Web version on PubMed Central for supplementary material.

ACKNOWLEDGMENTS

We thank Dr. Nicholas K. Conrad for kindly providing pcDNA3-METTL16, pcDNA3-METTL16-PP185/186AA, and METTL16-F187G and thank Dr. Johanna ten Hoeve-Scott for LC-MS data processing. This work was supported in part by the U.S. National Institutes of Health (NIH) grants R01 CA243386 (J.C.), R01 CA271497 (J.C.), R01 CA214965 (J.C.), R01 CA236399 (J.C.), R01 DK124116 (J.C), R01 CA233691 (C.C), R01 CA236626 (C.C), T32 CA186895 (B.T), The Simms/Mann Family Foundation (J.C.), The Margaret E. Early Medical Research Trust (R. S.), and The Leukemia Research Foundation (R.S.). J.C. is a Leukemia & Lymphoma Society (LLS) Scholar.

REFERENCES

1. Dohner H, Weisdorf DJ, and Bloomfield CD (2015). Acute Myeloid Leukemia. N Engl J Med 373, 1136–1152. 10.1056/NEJMra1406184. [PubMed: 26376137]
2. Hope KJ, Jin L, and Dick JE (2004). Acute myeloid leukemia originates from a hierarchy of leukemic stem cell classes that differ in self-renewal capacity. Nature immunology 5, 738–743. 10.1038/ni1080. [PubMed: 15170211]
3. Pollyea DA, and Jordan CT (2017). Therapeutic targeting of acute myeloid leukemia stem cells. Blood 129, 1627–1635. 10.1182/blood-2016-10-696039 [PubMed: 28159738]
4. Stubbs MC, and Armstrong SA (2007). Therapeutic implications of leukemia stem cell development. Clin Cancer Res 13, 3439–3442. [PubMed: 17575205]

5. Krivtsov AV, Twomey D, Feng Z, Stubbs MC, Wang Y, Faber J, Levine JE, Wang J, Hahn WC, Gilliland DG, et al. (2006). Transformation from committed progenitor to leukaemia stem cell initiated by MLL-AF9. Nature 442, 818–822. 10.1038/nature04980. [PubMed: 16862118]
6. Chen J, Odenike O, and Rowley JD (2010). Leukaemogenesis: more than mutant genes. Nat Rev Cancer 10, 23–36.10.1038/nrc2765. [PubMed: 20029422]
7. Ward PS, and Thompson CB (2012). Metabolic reprogramming: a cancer hallmark even warburg did not anticipate. Cancer Cell 21, 297–308. 10.1016/j.ccr.2012.02.014. [PubMed: 22439925]
8. Martinez-Reyes I, and Chandel NS (2021). Cancer metabolism: looking forward. Nat Rev Cancer 21, 669–680. 10.1038/s41568-021-00378-6. [PubMed: 34272515]
9. Boroughs LK, and DeBerardinis RJ (2015). Metabolic pathways promoting cancer cell survival and growth. Nature cell biology 17, 351–359. 10.1038/ncb3124. [PubMed: 25774832]
10. Gu Z, Liu Y, Cai F, Patrick M, Zmajkovic J, Cao H, Zhang Y, Tasdogan A, Chen M, Qi L, et al. (2019). Loss of EZH2 Reprograms BCAA Metabolism to Drive Leukemic Transformation. Cancer Discov 9, 1228–1247. 10.1158/2159-8290.cd-19-0152. [PubMed: 31189531]
11. Raffel S, Falcone M, Kneisel N, Hansson J, Wang W, Lutz C, Bullinger L, Poschet G, Nonnenmacher Y, Barnert A, et al. (2017). BCAT1 restricts alphaKG levels in AML stem cells leading to IDHmut-like DNA hypermethylation. Nature 551, 384–388. 10.1038/nature24294. [PubMed: 29144447]
12. Hattori A, Tsunoda M, Konuma T, Kobayashi M, Nagy T, Glushka J, Tayyari F, McSkimming D, Kannan N, Tojo A, et al. (2017). Cancer progression by reprogrammed BCAA metabolism in myeloid leukaemia. Nature 545, 500–504. 10.1038/nature22314. [PubMed: 28514443]
13. Brosnan JT, and Brosnan ME (2006). Branched-chain amino acids: enzyme and substrate regulation. The Journal of nutrition 136, 207S–211S. 10.1093/jn/136.1.207S. [PubMed: 16365084]
14. Harper AE, Miller RH, and Block KP (1984). Branched-chain amino acid metabolism. Annual review of nutrition 4, 409–454. 10.1146/annurev.nu.04.070184.002205.
15. Huang H, Weng H, and Chen J (2020). m(6)A Modification in Coding and Non-coding RNAs: Roles and Therapeutic Implications in Cancer. Cancer Cell 37, 270–288. 10.1016/j.ccell.2020.02.004. [PubMed: 32183948]
16. Deng X, Su R, Weng H, Huang H, Li Z, and Chen J (2018). RNA N(6)-methyladenosine modification in cancers: current status and perspectives. Cell Res 28, 507–517. 10.1038/s41422-018-0034-6. [PubMed: 29686311]
17. Qing Y, Su R, and Chen J (2021). RNA modifications in hematopoietic malignancies: a new research frontier. Blood 138, 637–648. 10.1182/blood.2019004263. [PubMed: 34157073]
18. Barbieri I, Tzelepis K, Pandolfini L, Shi J, Millan-Zambrano G, Robson SC, Aspris D, Migliori V, Bannister AJ, Han N, et al. (2017). Promoter-bound METTL3 maintains myeloid leukaemia by m(6)A-dependent translation control. Nature 552, 126–131. 10.1038/nature24678. [PubMed: 29186125]
19. Vu LP, Pickering BF, Cheng Y, Zaccara S, Nguyen D, Minuesa G, Chou T, Chow A, Saletore Y, MacKay M, et al. (2017). The N(6)-methyladenosine (m(6)A)-forming enzyme METTL3 controls myeloid differentiation of normal hematopoietic and leukemia cells. Nat Med 23, 1369–1376. 10.1038/nm.4416. [PubMed: 28920958]
20. Su R, Dong L, Li C, Nachtergaele S, Wunderlich M, Qing Y, Deng X, Wang Y, Weng X, Hu C, et al. (2018). R-2HG Exhibits Anti-tumor Activity by Targeting FTO/m(6)A/MYC/CEBPA Signaling. Cell 172, 90–105 e123. 10.1016/j.cell.2017.11.031. [PubMed: 29249359]
21. Bansal H, Yihua Q, Iyer SP, Ganapathy S, Proia DA, Penalva LO, Uren PJ, Suresh U, Carew JS, Karnad AB, et al. (2014). WTAP is a novel oncogenic protein in acute myeloid leukemia. Leukemia 28, 1171–1174. 10.1038/leu.2014.16. [PubMed: 24413322]
22. Qing Y, Dong L, Gao L, Li C, Li Y, Han L, Prince E, Tan B, Deng X, Wetzel C, et al. (2021). R-2-hydroxyglutarate attenuates aerobic glycolysis in leukemia by targeting the FTO/m(6)A/PFKP/LDHB axis. Mol Cell 81, 922–939 e929. 10.1016/j.molcel.2020.12.026. [PubMed: 33434505]
23. Wang J, Li Y, Wang P, Han G, Zhang T, Chang J, Yin R, Shan Y, Wen J, Xie X, et al. (2020). Leukemogenic Chromatin Alterations Promote AML Leukemia Stem Cells via a KDM4C-ALKBH5-AXL Signaling Axis. Cell stem cell 27, 81–97 e88. 10.1016/j.stem.2020.04.001. [PubMed: 32402251]

24. Paris J, Morgan M, Campos J, Spencer GJ, Shmakova A, Ivanova I, Mapperley C, Lawson H, Wotherspoon DA, Sepulveda C, et al. (2019). Targeting the RNA m(6)A Reader YTHDF2 Selectively Compromises Cancer Stem Cells in Acute Myeloid Leukemia. Cell Stem Cell 25, 137–148 e136. 10.1016/j.stem.2019.03.021. [PubMed: 31031138]
25. Cheng Y, Xie W, Pickering BF, Chu KL, Savino AM, Yang X, Luo H, Nguyen DT, Mo S, Barin E, et al. (2021). N(6)-Methyladenosine on mRNA facilitates a phase-separated nuclear body that suppresses myeloid leukemic differentiation. Cancer Cell 39, 958–972 e958. 10.1016/j.ccell.2021.04.017. [PubMed: 34048709]
26. Sheng Y, Wei J, Yu F, Xu H, Yu C, Wu Q, Liu Y, Li L, Cui XL, Gu X, et al. (2021). A Critical Role of Nuclear m6A Reader YTHDC1 in Leukemogenesis by Regulating MCM Complex-Mediated DNA Replication. Blood. 10.1182/blood.2021011707.
27. Huang H, Weng H, Deng X, and Chen J (2020). RNA modifications in cancer: functions, mechanisms, and therapeutic implications. Annual Review of Cancer Biology 4, 221–240.
28. Weng H, Huang H, Wu H, Qin X, Zhao BS, Dong L, Shi H, Skibbe J, Shen C, Hu C, et al. (2018). METTL14 Inhibits Hematopoietic Stem/Progenitor Differentiation and Promotes Leukemogenesis via mRNA m(6)A Modification. Cell Stem Cell 22, 191–205 e199. 10.1016/j.stem.2017.11.016. [PubMed: 29290617]
29. Shen C, Sheng Y, Zhu A, Robinson S, Jiang X, Dong L, Chen H, Su R, Yin Z, Li W, et al. (2020). RNA demethylase ALKBH5 selectively promotes tumorigenesis and cancer stem cell self-renewal in acute myeloid leukemia. Cell stem cell 27, 64–80. [PubMed: 32402250]
30. Brown JA, Kinzig CG, DeGregorio SJ, and Steitz JA (2016). Methyltransferase-like protein 16 binds the 3'-terminal triple helix of MALAT1 long noncoding RNA. Proc Natl Acad Sci U S A 113, 14013–14018. 10.1073/pnas.1614759113. [PubMed: 27872311]
31. Pendleton KE, Chen B, Liu K, Hunter OV, Xie Y, Tu BP, and Conrad NK (2017). The U6 snRNA m(6)A Methyltransferase METTL16 Regulates SAM Synthetase Intron Retention. Cell 169, 824–835 e814. 10.1016/j.cell.2017.05.003. [PubMed: 28525753]
32. Warda AS, Kretschmer J, Hackert P, Lenz C, Urlaub H, Hobartner C, Sloan KE, and Bohnsack MT (2017). Human METTL16 is a N(6)-methyladenosine (m(6)A) methyltransferase that targets pre-mRNAs and various non-coding RNAs. EMBO Rep 18, 2004–2014. 10.15252/embr.201744940. [PubMed: 29051200]
33. Shima H, Matsumoto M, Ishigami Y, Ebina M, Muto A, Sato Y, Kumagai S, Ochiai K, Suzuki T, and Igarashi K (2017). S-Adenosylmethionine Synthesis Is Regulated by Selective N(6)-Adenosine Methylation and mRNA Degradation Involving METTL16 and YTHDC1. Cell Rep 21, 3354–3363. 10.1016/j.celrep.2017.11.092. [PubMed: 29262316]
34. Mendel M, Chen KM, Homolka D, Gos P, Pandey RR, McCarthy AA, and Pillai RS (2018). Methylation of Structured RNA by the m(6)A Writer METTL16 Is Essential for Mouse Embryonic Development. Mol Cell 71, 986–1000 e1011. 10.1016/j.molcel.2018.08.004. [PubMed: 30197299]
35. Doxtader KA, Wang P, Scarborough AM, Seo D, Conrad NK, and Nam Y (2018). Structural Basis for Regulation of METTL16, an S-Adenosylmethionine Homeostasis Factor. Mol Cell 71, 1001–1011 e1004. 10.1016/j.molcel.2018.07.025. [PubMed: 30197297]
36. Su R, Dong L, Li Y, Gao M, He PC, Liu W, Wei J, Zhao Z, Gao L, Han L, et al. (2022). METTL16 exerts an m(6)A-independent function to facilitate translation and tumorigenesis. Nat Cell Biol 24, 205–216. 10.1038/s41556-021-00835-2. [PubMed: 35145225]
37. Aoyama T, Yamashita S, and Tomita K (2020). Mechanistic insights into m6A modification of U6 snRNA by human METTL16. Nucleic acids research 48, 5157–5168. 10.1093/nar/gkaa227. [PubMed: 32266935]
38. Wong JM, and Eirin-Lopez JM (2021). Evolution of Methyltransferase-Like (METTL) Proteins in Metazoa: A Complex Gene Family Involved in Epitranscriptomic Regulation and Other Epigenetic Processes. Mol Biol Evol 38, 5309–5327. 10.1093/molbev/msab267. [PubMed: 34480573]
39. Petrossian TC, and Clarke SG (2011). Uncovering the human methyltransferasome. Mol Cell Proteomics 10, M110 000976. 10.1074/mcp.M110.000976.

40. Tsherniak A, Vazquez F, Montgomery PG, Weir BA, Kryukov G, Cowley GS, Gill S, Harrington WF, Pantel S, Krill-Burger JM, et al. (2017). Defining a Cancer Dependency Map. Cell 170, 564–576 e516. 10.1016/j.cell.2017.06.010. [PubMed: 28753430]
41. Yan M, Kanbe E, Peterson LF, Boyapati A, Miao Y, Wang Y, Chen IM, Chen Z, Rowley JD, Willman CL, and Zhang DE (2006). A previously unidentified alternatively spliced isoform of t(8;21) transcript promotes leukemogenesis. Nat Med 12, 945–949. [PubMed: 16892037]
42. Somervaille TC, and Cleary ML (2006). Identification and characterization of leukemia stem cells in murine MLL-AF9 acute myeloid leukemia. Cancer Cell 10, 257–268. [PubMed: 17045204]
43. Su R, Dong L, Li Y, Gao M, Han L, Wunderlich M, Deng X, Li H, Huang Y, Gao L, et al. (2020). Targeting FTO Suppresses Cancer Stem Cell Maintenance and Immune Evasion. Cancer cell 38, 79–96 e11. 10.1016/j.ccell.2020.04.017. [PubMed: 32531268]
44. Zhang C, Chen Y, Sun B, Wang L, Yang Y, Ma D, Lv J, Heng J, Ding Y, Xue Y, et al. (2017). m(6)A modulates haematopoietic stem and progenitor cell specification. Nature 549, 273–276. 10.1038/nature23883. [PubMed: 28869969]
45. Lee H, Bao S, Qian Y, Geula S, Leslie J, Zhang C, Hanna JH, and Ding L (2019). Stage-specific requirement for Mett13-dependent m6A mRNA methylation during haematopoietic stem cell differentiation. Nature cell biology 21, 700–709. 10.1038/s41556-019-0318-1. [PubMed: 31061465]
46. Cheng Y, Luo H, Izzo F, Pickering BF, Nguyen D, Myers R, Schurer A, Gourkanti S, Brüning JC, Vu LP, et al. (2019). m6A RNA Methylation Maintains Hematopoietic Stem Cell Identity and Symmetric Commitment. Cell Rep 28, 1703–1716.e1706. [PubMed: 31412241]
47. Yao QJ, Sang L, Lin M, Yin X, Dong W, Gong Y, and Zhou BO (2018). Mettl3-Mettl14 methyltransferase complex regulates the quiescence of adult hematopoietic stem cells. Cell Res 28, 952–954. 10.1038/s41422-018-0062-2. [PubMed: 30006613]
48. Li Z, Qian P, Shao W, Shi H, He XC, Gogol M, Yu Z, Wang Y, Qi M, Zhu Y, et al. (2018). Suppression of m6A reader Ythdf2 promotes hematopoietic stem cell expansion. Cell Research 28, 904–917. 10.1038/s41422-018-0072-0. [PubMed: 30065315]
49. Wang H, Zuo H, Liu J, Wen F, Gao Y, Zhu X, Liu B, Xiao F, Wang W, Huang G, et al. (2018). Loss of YTHDF2-mediated m6A-dependent mRNA clearance facilitates hematopoietic stem cell regeneration. Cell Research 28, 1035–1038. 10.1038/s41422-018-0082-y. [PubMed: 30150673]
50. Subramanian A, Tamayo P, Mootha VK, Mukherjee S, Ebert BL, Gillette MA, Paulovich A, Pomeroy SL, Golub TR, Lander ES, and Mesirov JP (2005). Gene set enrichment analysis: a knowledge-based approach for interpreting genome-wide expression profiles. Proceedings of the National Academy of Sciences of the United States of America 102, 15545–15550. 10.1073/pnas.0506580102. [PubMed: 16199517]
51. Yoon I, Nam M, Kim HK, Moon HS, Kim S, Jang J, Song JA, Jeong SJ, Kim SB, Cho S, et al. (2020). Glucose-dependent control of leucine metabolism by leucyl-tRNA synthetase 1. Science 367, 205–210. 10.1126/science.aau2753. [PubMed: 31780625]
52. Tonjes M, Barbus S, Park YJ, Wang W, Schlotter M, Lindroth AM, Pleier SV, Bai AHC, Karra D, Piro RM, et al. (2013). BCAT1 promotes cell proliferation through amino acid catabolism in gliomas carrying wild-type IDH1. Nat Med 19, 901–908. 10.1038/nm.3217. [PubMed: 23793099]
53. Huang H, Weng H, Sun W, Qin X, Shi H, Wu H, Zhao BS, Mesquita A, Liu C, Yuan CL, et al. (2018). Recognition of RNA N(6)-methyladenosine by IGF2BP proteins enhances mRNA stability and translation. Nat Cell Biol 20, 285–295. 10.1038/s41556-018-0045-z. [PubMed: 29476152]
54. Sheng Y, Wei J, Yu F, Xu H, Yu C, Wu Q, Liu Y, Li L, Cui XL, Gu X, et al. (2021). A critical role of nuclear m6A reader YTHDC1 in leukemogenesis by regulating MCM complex-mediated DNA replication. Blood 138, 2838–2852. 10.1182/blood.2021011707. [PubMed: 34255814]
55. Weng H, Huang F, Yu Z, Chen Z, Prince E, Kang Y, Zhou K, Li W, Hu J, Fu C, et al. (2022). The m(6)A reader IGF2BP2 regulates glutamine metabolism and represents a therapeutic target in acute myeloid leukemia. Cancer Cell. 10.1016/j.ccell.2022.10.004.
56. Biswas D, Duffley L, and Pulinilkunnil T (2019). Role of branched-chain amino acid-catabolizing enzymes in intertissue signaling, metabolic remodeling, and energy homeostasis. FASEB J 33, 8711–8731. 10.1096/fj.201802842RR. [PubMed: 31084571]

57. Lee H, Bao S, Qian Y, Geula S, Leslie J, Zhang C, Hanna JH, and Ding L (2019). Stage-specific requirement for Mettl3-dependent m(6)A mRNA methylation during haematopoietic stem cell differentiation. Nat Cell Biol 21, 700–709. 10.1038/s41556-019-0318-1. [PubMed: 31061465]
58. Cheng Y, Luo H, Izzo F, Pickering BF, Nguyen D, Myers R, Schurer A, Gourkanti S, Bruning JC, Vu LP, et al. (2019). m(6)A RNA Methylation Maintains Hematopoietic Stem Cell Identity and Symmetric Commitment. Cell Rep 28, 1703–1716 e1706. 10.1016/j.celrep.2019.07.032. [PubMed: 31412241]
59. Yankova E, Blackaby W, Albertella M, Rak J, De Braekeleer E, Tsagkogeorga G, Pilka ES, Aspris D, Leggate D, Hendrick AG, et al. (2021). Small-molecule inhibition of METTL3 as a strategy against myeloid leukaemia. Nature 593, 597–601. 10.1038/s41586-021-03536-w. [PubMed: 33902106]
60. Campeau E, Ruhl VE, Rodier F, Smith CL, Rahmberg BL, Fuss JO, Campisi J, Yaswen P, Cooper PK, and Kaufman PD (2009). A versatile viral system for expression and depletion of proteins in mammalian cells. PloS one 4, e6529. 10.1371/journal.pone.0006529. [PubMed: 19657394]
61. Stewart SA, Dykxhoorn DM, Palliser D, Mizuno H, Yu EY, An DS, Sabatini DM, Chen IS, Hahn WC, Sharp PA, et al. (2003). Lentivirus-delivered stable gene silencing by RNAi in primary cells. RNA 9, 493–501. 10.1261/rna.2192803. [PubMed: 12649500]
62. Stringer BW, Day BW, D'Souza RCJ, Jamieson PR, Ensbey KS, Bruce ZC, Lim YC, Goasdoue K, Offenhauser C, Akgul S, et al. (2019). A reference collection of patient-derived cell line and xenograft models of proneural, classical and mesenchymal glioblastoma. Sci Rep 9, 4902. 10.1038/s41598-019-41277-z. [PubMed: 30894629]
63. Sanjana NE, Shalem O, and Zhang F (2014). Improved vectors and genome-wide libraries for CRISPR screening. Nat Methods 11, 783–784. 10.1038/nmeth.3047. [PubMed: 25075903]
64. Naviaux RK, Costanzi E, Haas M, and Verma IM (1996). The pCL vector system: rapid production of helper-free, high-titer, recombinant retroviruses. J Virol 70, 5701–5705. 10.1128/JVI.70.8.5701-5705.1996. [PubMed: 8764092]
65. Li B, and Dewey CN (2011). RSEM: accurate transcript quantification from RNA-Seq data with or without a reference genome. BMC Bioinformatics 12, 323. 10.1186/1471-2105-12-323. [PubMed: 21816040]
66. Dobin A, Davis CA, Schlesinger F, Drenkow J, Zaleski C, Jha S, Batut P, Chaisson M, and Gingeras TR (2013). STAR: ultrafast universal RNA-seq aligner. Bioinformatics 29, 15–21. 10.1093/bioinformatics/bts635. [PubMed: 23104886]
67. Wunderlich M, Mizukawa B, Chou FS, Sexton C, Shrestha M, Saunthararajah Y, and Mulloy JC (2013). AML cells are differentially sensitive to chemotherapy treatment in a human xenograft model. Blood 121, e90–97. 10.1182/blood-2012-10-464677. [PubMed: 23349390]
68. Doench JG, Fusi N, Sullender M, Hegde M, Vaimberg EW, Donovan KF, Smith I, Tothova Z, Wilen C, Orchard R, et al. (2016). Optimized sgRNA design to maximize activity and minimize off-target effects of CRISPR-Cas9. Nat Biotechnol 34, 184–191. 10.1038/nbt.3437. [PubMed: 26780180]
69. Li Z, Weng H, Su R, Weng X, Zuo Z, Li C, Huang H, Nachtergaele S, Dong L, Hu C, et al. (2017). FTO Plays an Oncogenic Role in Acute Myeloid Leukemia as a N(6)-Methyladenosine RNA Demethylase. Cancer cell 31, 127–141. 10.1016/j.ccell.2016.11.017. [PubMed: 28017614]
70. Jiang X, Hu C, Arnovitz S, Bugno J, Yu M, Zuo Z, Chen P, Huang H, Ulrich B, Gurbuxani S, et al. (2016). miR-22 has a potent anti-tumour role with therapeutic potential in acute myeloid leukaemia. Nature communications 7, 11452. 10.1038/ncomms11452.
71. Shen C, Sheng Y, Zhu AC, Robinson S, Jiang X, Dong L, Chen H, Su R, Yin Z, Li W, et al. (2020). RNA Demethylase ALKBH5 Selectively Promotes Tumorigenesis and Cancer Stem Cell Self-Renewal in Acute Myeloid Leukemia. Cell stem cell 27, 64–80 e69. 10.1016/j.stem.2020.04.009. [PubMed: 32402250]
72. Gu Z, Liu Y, Zhang Y, Cao H, Lyu J, Wang X, Wylie A, Newkirk SJ, Jones AE, Lee M Jr., et al. (2021). Silencing of LINE-1 retrotransposons is a selective dependency of myeloid leukemia. Nature genetics 53, 672–682. 10.1038/s41588-021-00829-8. [PubMed: 33833453]

73. Carreer WJ, Flight RM, and Moseley HN (2013). A Computational Framework for High-Throughput Isotopic Natural Abundance Correction of Omics-Level Ultra-High Resolution FT-MS Datasets. Metabolites 3. 10.3390/metabo3040853.

74. Moseley HN (2010). Correcting for the effects of natural abundance in stable isotope resolved metabolomics experiments involving ultra-high resolution mass spectrometry. BMC Bioinformatics 11, 139. 10.1186/1471-2105-11-139. [PubMed: 20236542]

Highlights

- CRISPR-Cas9 screening reveals the robust dependency of METTL16 in AML
- METTL16 is required for AML development/maintenance and LSC/LIC self-renewal
- *BCAT1* and *BCAT2* are two *bona-fide* m^6A-dependent essential targets of METTL16 in AML
- METTL16 promotes leukemogenesis & LCS/LIC self-renewal via rewiring BCAA metabolism

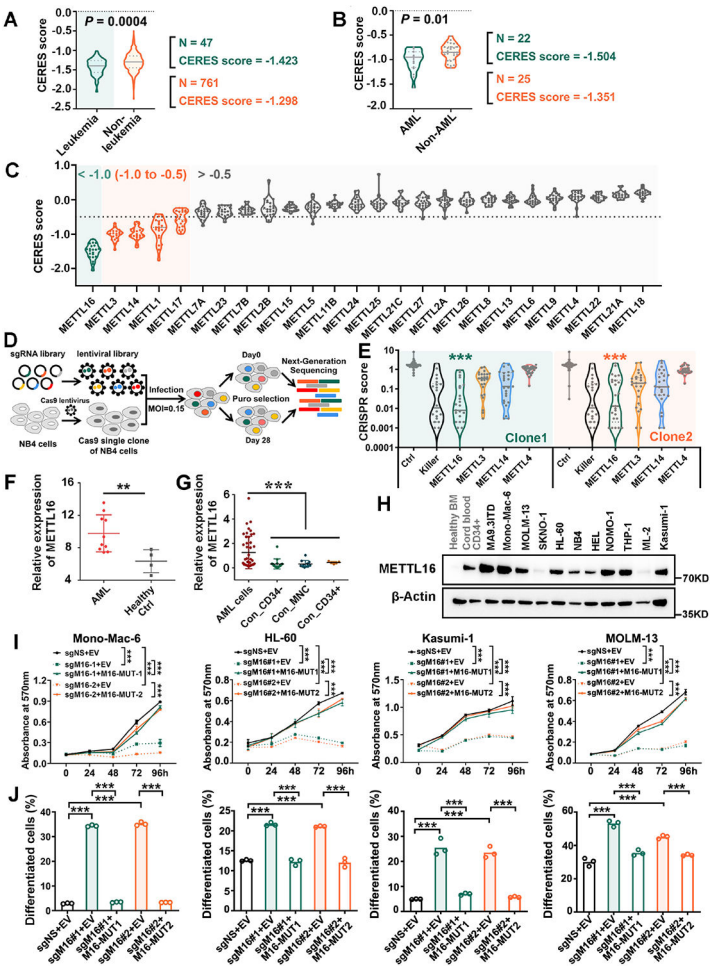

Figure 1. CRISPR-Cas9 Screenings and *in vitro* Functional Studies Reveal the Dependency of METTL16 for AML Cell Survival and Proliferation.

(A) Comparison of METTL16 CERES scores between the 47 leukemia cell lines and the 761 non-leukemia cell lines.

(B) Comparison of METTL16 CERES scores between the 22 AML cell lines and the 25 non-AML leukemia cell lines.

(C) Violin plots depicting the CERES scores of all the METTL family members across the 22 AML cell lines.

(D) Schematic describing our in-house CRISPR screening in two NB4 cas9 single clones.

(E) Violin plots presenting the CRISPR scores of indicated gene in two NB4 cas9 single clones. Killer gene was served as a positive control. The *** ($p < 0.001$) represents the p values of unpaired *t* test of METTL16 vs. Ctrl, METTL16 vs. METTL3, METTL16 vs. METTL14, and METTL16 vs. METTL4 (n=25 sgRNAs).

(F) Comparison of expression levels of *METTL16* between AML samples (n=10 patients) and healthy controls (n=4 healthy donors) as determined by RNA-seq (mean ± SD).

(G) Relative expression levels of *METTL16* in human AML samples (n=45 cell lines), healthy MNC (n=16 healthy donors), healthy MNC-derived $CD34^-$ cells (n=11 healthy donors) and healthy MNC-derived CD34+ cells (n=5 healthy donors) as determined by qPCR (mean ± SD).

(H) Western blotting showing expression of METTL16 in AML cells (n=11 cell lines) and healthy controls. β-actin was used as a loading control.
(I, J) The effects of *METTL16* KO with or without METTL16 restoration on the proliferation/growth (I; detected by MTT assay) and myeloid differentiation (J; detected by flow cytometry) of human AML cell lines (mean ± SD, n = 3 independent experiments). Statistical analysis: Unpaired *t* test (A, B, E, F, and G); Two-way ANOVA (I); One-way ANOVA (J). **p < 0.01; ***p < 0.001. See also Figure S1.

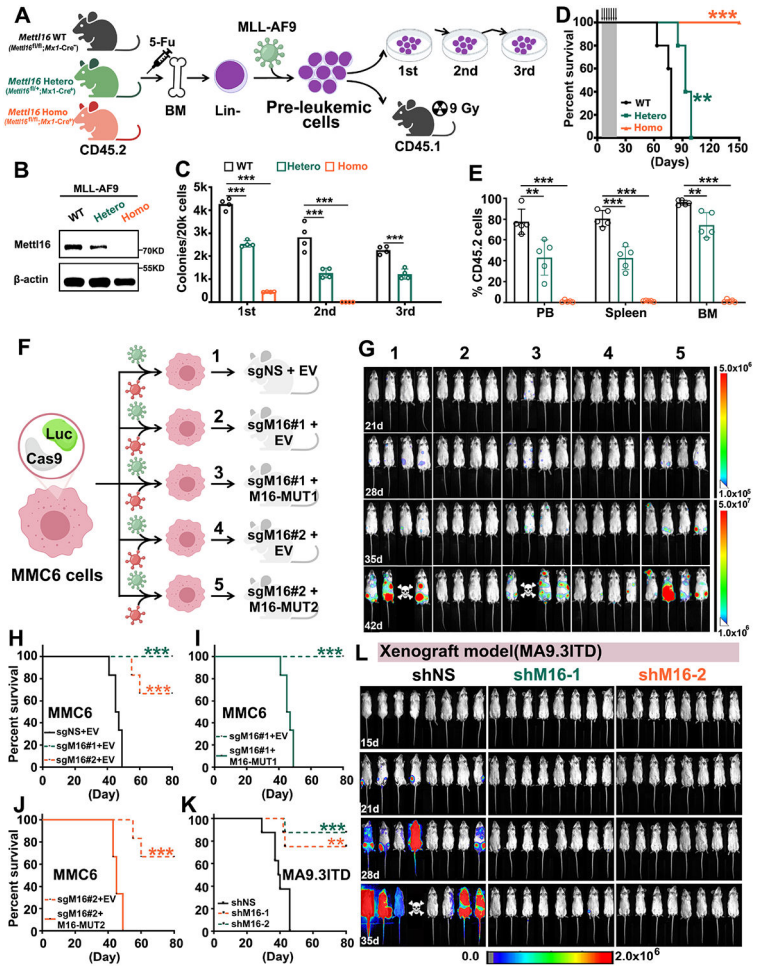

Figure 2. METTL16 is Required for Leukemogenesis *in vivo*.

(A) Schematic overview of *in vivo* primary bone marrow transplantation (BMT) assay and *in vitro* colony-forming/replating assay (CFA).

(B) Western blot confirming depletion of *Mettl16* in MA9-transduced murine Lin$^-$ HSPCs.

(C) Effect of *Mettl*16 KO on the colony forming ability of MA9-transduced Lin$^-$ HSPCs. Data are represented as mean ± SD (n = 4 independent experiments).

(D) Kaplan-Meier survival curves of mice transplanted with MA9 transduced WT, *Mettl16* Hetero, and *Mettl16* Homo Lin$^-$ HSPCs (n = 5 mice per group).

(E) Percentage of the MA9 AML donor cells (CD45.2$^+$) in the PB, spleen, and BM of primary BMT recipient mice (CD45.1$^+$). The samples were collected on day 78 post transplantation. (mean ± SD, n = 5 mice per group)

(F) Schematic of xenotransplantation assay with human AML cells and NRGS immune-deficient recipient mice.

(G) Representative *in vivo* bioluminescent images of NRGS recipient mice xeno-transplanted with luciferase$^+$/Cas9$^+$ MMC6 AML cells transduced with indicated lentiviruses (see Figure 2F for the annotation).

(H-J) Kaplan-Meier survival curves of NRGS recipient mice xeno-transplanted with luciferase$^+$/Cas9$^+$ MMC6 cells transduced with indicated lentiviruses. n = 6 mice per group.

(K) Kaplan-Meier survival curves of NRGS recipient mice xeno-transplanted with luciferase^{+} MA9.3ITD AML cells that were virally transduced with indicated lentiviruses. n = 8 mice per group.

(L) *In vivo* bioluminescent images of NRGS recipient mice xeno-transplanted with luciferase^{+} MA9.3ITD cells transduced with indicated lentiviruses. n= 8 mice per group. Statistical analysis: Log-rank test (D, and H-K); Unpaired *t* test (C and E). *p < 0.05; **p < 0.01; ***p < 0.001. See also Figure S2.

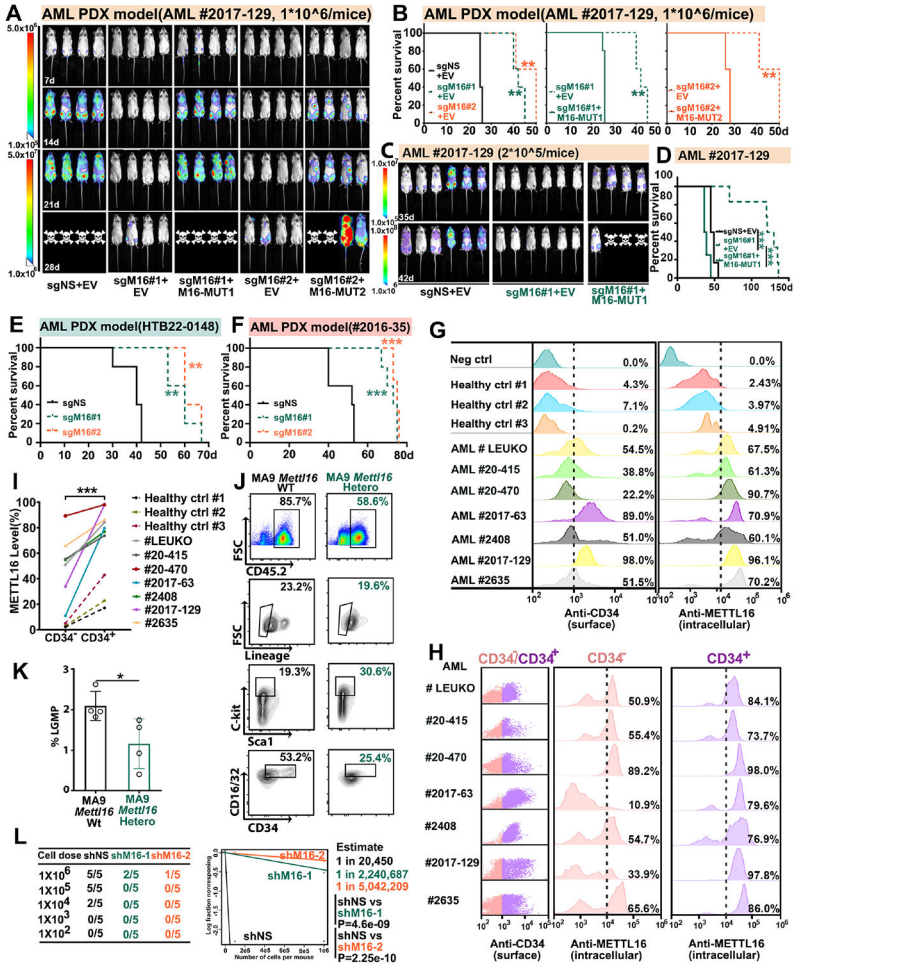

Figure 3. METTL16 is highly Expressed in LSCs/LICs and Genetic Depletion of *METTL16* Attenuates LSC/LIC Self-renewal.

(A) *In vivo* bioluminescent images of PDX mouse models with human AML 2017-129 cells (1×10^6 per recipient) transduced with indicated lentiviruses.

(B) Kaplan-Meier curves showing the effect of *METTL16* KO alone or with restored *METTL16* expression on the survival of AML 2017-129 PDX models (1×10^6 per recipient). n = 5 mice per group.

(C) *In vivo* bioluminescent images of AML 2017-129 PDX models upon *METTL16* KO (2×10^5 per recipient).

(D) Kaplan-Meier curves showing the effect of *METTL16* level changes on survival of AML 2017-129 PDX models (2×10^5 per recipient). n = 6 mice for sgNS+EV; n = 6 mice for sgM16-1+EV; n = 4 mice for sgM16-2+M16-MUT1.

(E, F) Kaplan-Meier curves showing the effect of *METTL16* KO on the survival of AML HTB22-0148 (E) and 2016-35 (F) PDX models (5×10^6 per recipient). n = 5 mice per group.

(G) Histogram Plot showing CD34 surface staining and METTL16 intracellular staining in bulk BM-derived mononuclear cells (BMMNCs) of healthy donors (n = 3) and AML patients (n = 7).

(H) Histogram Plot showing METTL16 abundance in $CD34^-$ and $CD34^+$ population in BM cells from AML patients (n = 7).

(I) Comparison of METTL16 abundance between paired $CD34^-$ and $CD34^+$ BMMNCs from AML patients and healthy control donors (n = 10).
(J) Scheme depicting the gating strategy for GMP-L LSC population in BM MNCs of primary MA9 AML mice. The representative data from *Mettl16* WT and heterozygous KO groups were shown. The samples were collected on 78 days post BMT.
(K) Percentage of GMP-L LSCs in the BM of *Mettl16* WT and $Mettl16^{fl/+}$ MA9 AML mice (mean ± SD, n = 4 mice per group).
(L) *In vivo* limiting dilution assay showing the effect of *Mettl16* depletion on LSC frequency. Table (left panel) shows the donor cell numbers used for secondary MA9 BMT and the ratios of the recipient mice with AML symptom 8 weeks post transplantation. Graph (right panel) shows LSC/LIC frequency, and the p values as determined by ELDA software. n = 5 mice per group.
Statistical analysis: Log-rank test (B, D, E, and F); Paired *t* test (I); Unpaired *t* test (K). **p < 0.01; ***p < 0.001. See also Figure S3.

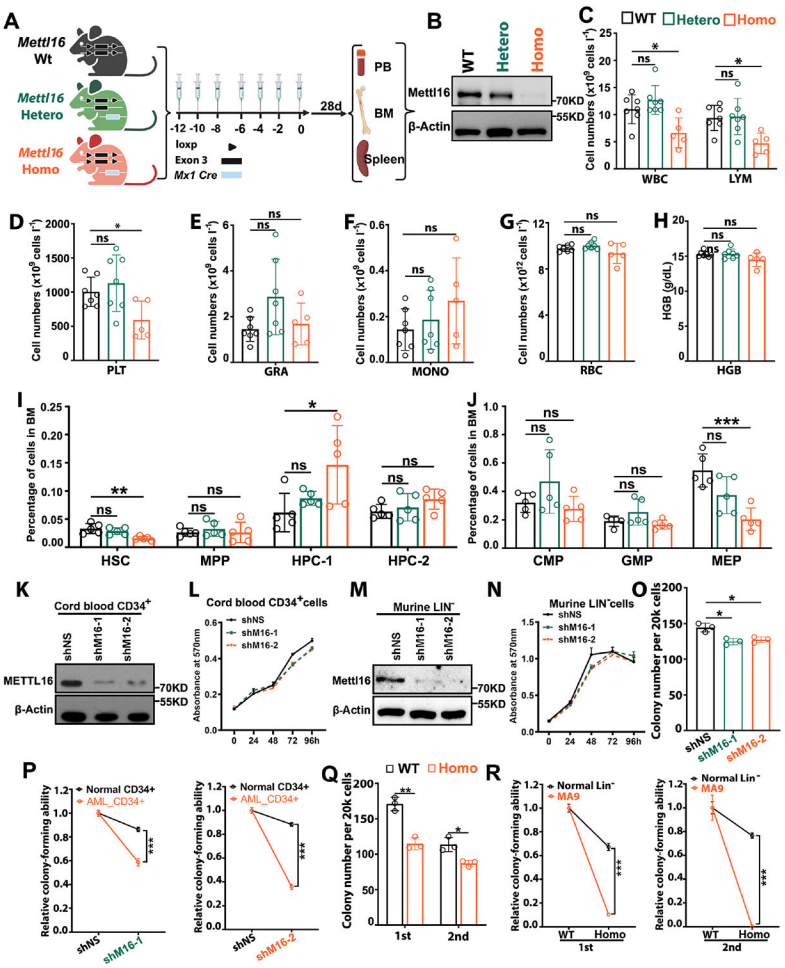

Figure 4. *METTL16* Deletion Shows Moderate Effect on Normal Hematopoiesis.

(A) Schematic overview of poly(I:C)-induced conditional KO of *Mettl16* in mice.

(B) Western blotting showing the *Mettl16* KO in murine Lin$^-$ HSPCs. The samples were collected 4 weeks post poly(I:C) treatment.

(C-H) PB analysis of *Mettl16* WT, heterozygous KO and homozygous KO mice. The PB samples were collected 4 weeks post poly(I:C) treatment. The levels of white blood cells (WBC) and lymphoma cells (LYM) (C), palates (PLT) (D), granulocytes (Granu) (E), Monocyte (MONO)

(F), Red blood cells (RBC) (G), and HGB (H) were displayed (mean ± SD) (n = 7 WT mice, n =7 heterozygous mice, n = 5 homozygous mice).

(I, J) Frequencies of various hematopoietic progenitors in the BM of *Mettl16* WT, heterozygous KO and homozygous KO mice. The PB samples were collected 4 weeks post poly(I:C) treatment (mean ± SD, n = 5 mice per group).

(K) Western blotting showing KD efficiency of *METTL16* shRNAs in human cord blood CD34$^+$ HSPCs.

(L) Effect of *METTL16* KD on cell proliferation/growth of human cord blood CD34$^+$ HSPCs (mean ± SD, n = 3 independent experiments).

(M) Western blotting showing KD efficiency of *Mettl16* shRNAs in murine Lin$^-$ HSPCs.

(N) Effect of *Mettl16* KD on cell proliferation/growth of murine Lin^- HSPCs (mean ± SD, n = 3 independent experiments)
(O) Effect of *METTL16* KD on the colony-forming ability of human normal BM $CD34^+$ HSPCs (mean ± SD, n = 3 independent experiments).
(P) Comparison of the effects of *METTL16* KD on the colony-forming ability between human normal BM $CD34^+$ HSPCs and AML BM $CD34^+$ LSCs/LICs.
(Q) Effect of *Mettl16* deletion on the colony-forming ability of murine normal Lin^- HSPCs (mean ± SD, n = 3 independent experiments).
(R) Comparison of the effects of *Mettl16* deletion on the colony-forming ability between murine normal Lin^- HSPCs and AML MA9 LSCs/LICs (mean ± SD, n = 3 independent experiments).
Statistical analysis: Unpaired t test (C-J, O-R); Two-way ANOVA (L and N). **$p < 0.01$; ***$p < 0.001$. See also Figure S4.

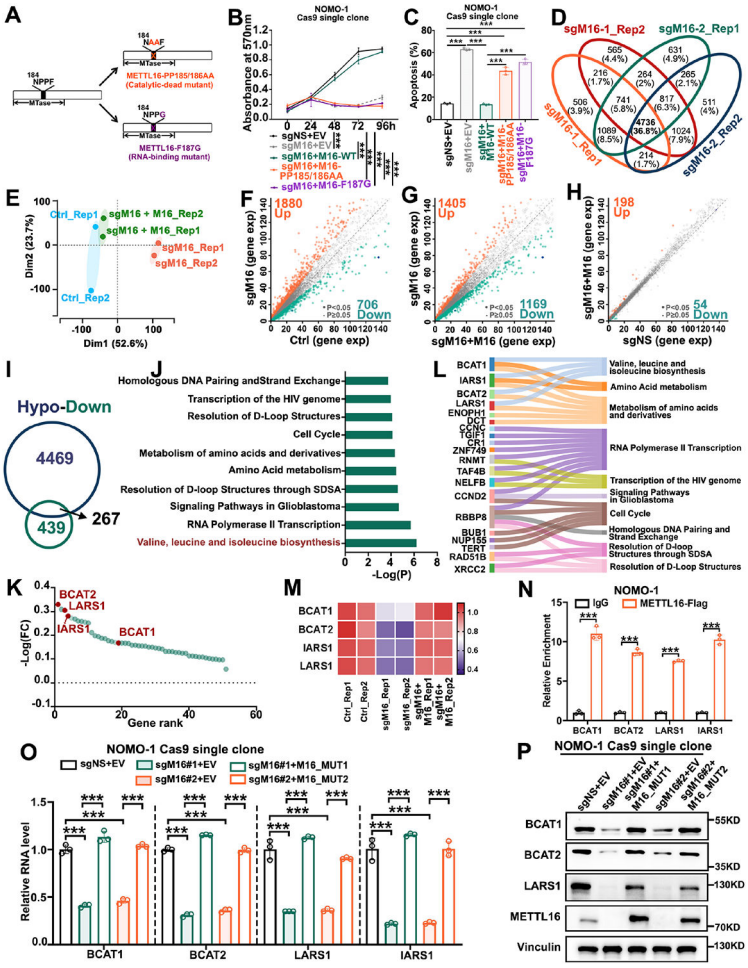

Figure 5. The Methyltransferase Activity of METTL16 is Required for its Tumor-Promoting Function in AML.

(A) Schematic representation of the location of mutations in the MTase-domain of METTL16. MTase-domain: Methyltransferase domain. PP185/186AA: Catalytic-dead mutant. F187G: RNA-binding mutant.

(B, C) Effect of restoration of WT or two loss-of-function mutants of METTL16 on cell proliferation/growth (B) or apoptosis (C) of NOMO-1 AML cells upon endogenous *METTL16* KO (mean ± SD, n = 3 independent experiments).

(D) MeRIP-seq analysis showing the overlap of m^{6}A-hypo transcripts in NOMO-1 cells upon two sgRNAs-mediated *METTL16* KO from two biological replicates. MeRIP-seq, m^{6}A specific methylated RNA immunoprecipitation.

(E) Principal component analysis (PCA) of RNA-seq data from the three groups of NOMO-1 cells (n = 2 biological replicates).

(F-H) Scatterplot showing the changes of gene expression between Ctrl and sgM16 groups (F), between sgM16+M16 and sgM16 groups (G), or between Ctrl and sgM16+M16 groups (H). Significantly upregulated and downregulated genes were highlighted in orange and green, respectively. FC, fold change.

(I) Venn diagram showing the overlap between the transcripts with m^6A-hypo peaks upon *METTL16* KO (MeRIP-seq) and the significantly downregulated transcripts upon *METTL16* KO (RNA-seq) in NOMO-1 cells.
(J) GSEA analysis of overlapping transcripts in Figure 5I. Top 10 significantly enriched pathways and the −log(P) value for each pathway were shown.
(K) Hockey-stick plot representing all the core enriched genes in the Top 10 significantly enriched pathways in Figure 5J. Genes were ranked according to their −logFC (Ctrl vs sgM16) values based on our RNA-seq results. The genes associated with Valine, leucine and isoleucine biosynthesis pathway are shown in red.
(L) Sankey diagram showing the top 20 down-regulated core enriched gene in Figure 5K and their corresponding pathways.
(M) Heatmap showing the expression levels of *BCAT1*, *BCAT2*, *LARS1* and *IARS1* in NOMO-1 cells transduced with indicated lentiviruses. The results were derived from our RNA-seq.
(N) RIP-qPCR analysis showing that METTL16 directly binds to *BCAT1*, *BCAT2*, *LARS1* and *IARS1* transcripts in NOMO-1 cells (mean ± SD, n = 3 independent experiments).
(O) qPCR analysis of *BCAT1*, *BCAT2*, *LARS1* and *IARS1* mRNA levels changes upon modulating METTL16 expression in NOMO-1 cells (mean ± SD, n = 3 independent experiments).
(P) Protein level changes of BCAT1, BCAT2 and LARS1 in NOMO-1 cells upon METTK16 KO with or without METTL16 restoration, as detected by Western blotting. For IARS1, we didn’t find an appropriate antibody to detect its expression.
Statistical analysis: Two-way ANOVA (B); One-way ANOVA (C and O); Unpaired t test (N). ***$p < 0.001$. See also Figure S5.

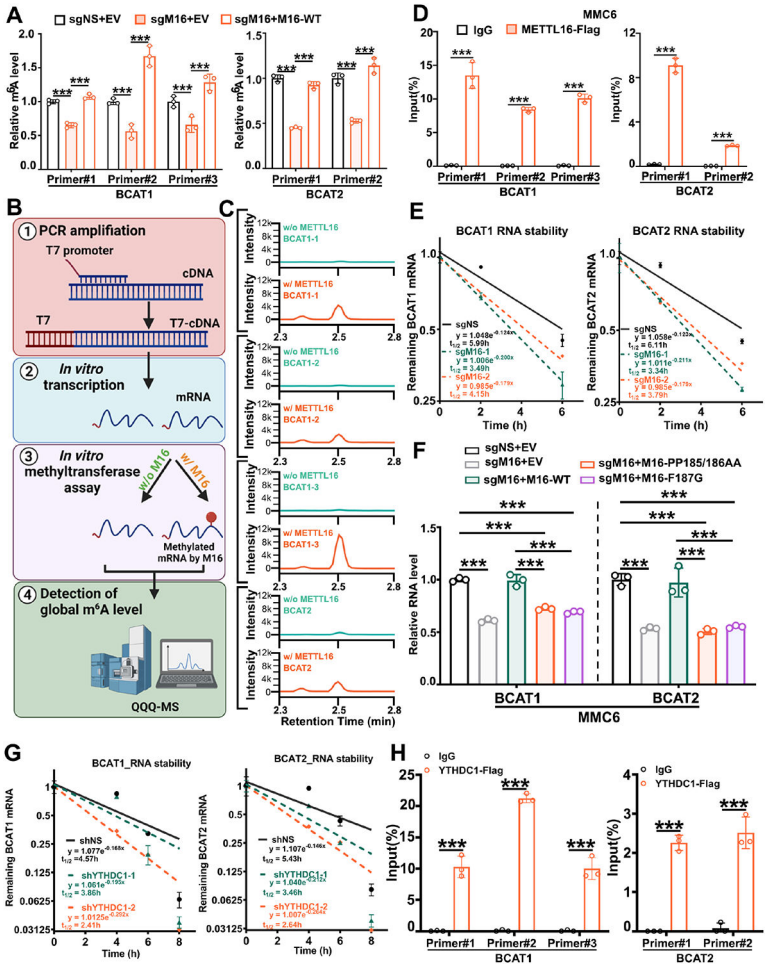

Figure 6. METTL16 positively Regulates *BCAT1* and *BCAT2* Expression in an m^{6}A-Dependent Manner.

(A) Gene-specific m^{6}A qPCR analysis of m^{6}A enrichment on *BCAT1* and *BCAT2* mRNA transcripts in MMC6 cells (mean ± SD, n = 3 independent experiments).

(B) Schematic describing the *in vitro* (cell-free) methyltransferase assays with recombinant METTL16 protein.

(C) Evaluation of the m^{6}A methyltransferase activity of METTL16 in methylating *BCAT1* and *BCAT2* mRNAs by QQQ-MS.

(D) METTL16 RIP-qPCR analysis showing METTL16 directly binds to *BCAT1* and *BCAT2* mRNA in MMC6 cells (mean ± SD, n = 3 independent experiments).

(E) The stability changes of *BCAT1* and *BCAT2* mRNAs in MMC6 cells upon *METTL16* KO (mean ± SD, n = 3 independent experiments).

(F) qPCR analysis of rescue effect of WT or catalytic inactive mutant (PP185/186AA and F187G) METTL16 on *BCAT1* and *BCAT2* expression in MMC6 cells with endogenous *METTL16* KO (mean ± SD, n = 3 independent experiments).

(G) Effect of *YTHDC1* KD on the stability of *BCAT1* (left panel) and *BCAT2* (right panel) mRNAs in MMC6 cells (mean ± SD, n = 3 independent experiments).

(H) Determination of the direct binding of YTHDC1 with *BCAT1*/*BCAT2* mRNA transcripts in MMC6 cells (mean ± SD, n = 3 independent experiments).

Statistical analysis: One-way ANOVA (A and F); Unpaired *t* test (D and H). **p < 0.01; ***p <0.001. See also Figure S6.

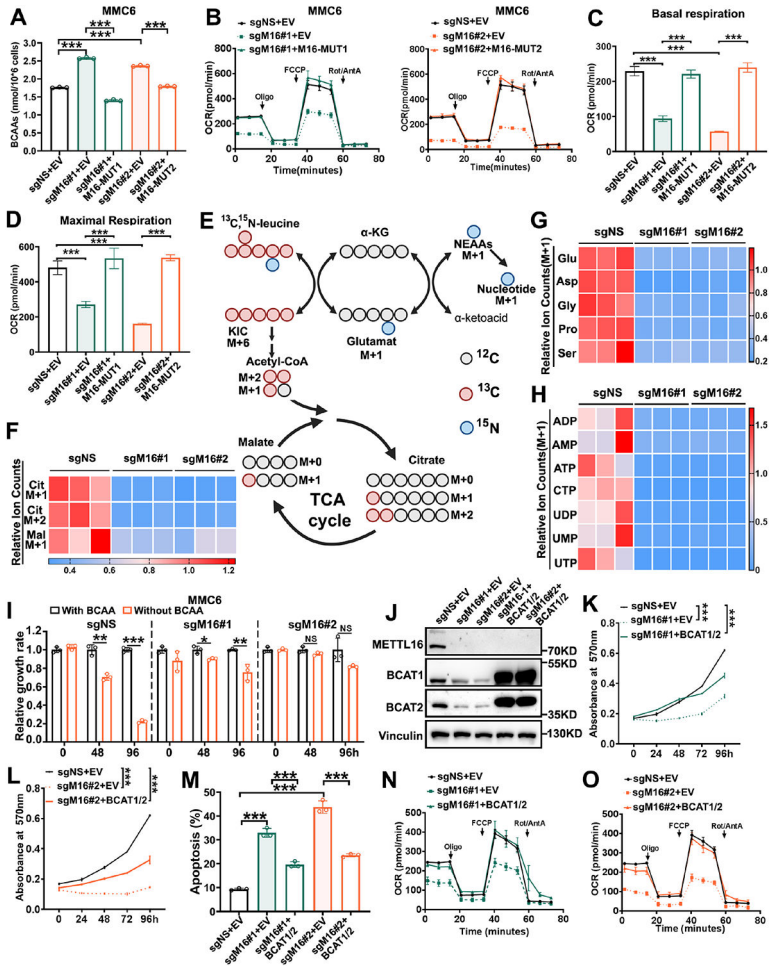

Figure 7. *METTL16* KO Subverts BCAA Metabolism in AML.

(A) Intracellular free BCAA concentration in MMC6 cells after transduction with indicated lentiviruses (mean ± SD, n = 3 independent experiments).

(B) Measurement of oxygen consumption rates (OCR) in MMC6 cells infected with indicated lentiviruses (mean ± SD, n = 4 independent experiments).

(C, D) Effect of METTL16 changes on basal (C) and maximal (D) respiration in MMC6 cells (mean ± SD, n = 4 independent experiments).

(E) Schematic outline of leucine tracing assay. Red circles indicate ^{13}C-labeled carbons. Blue circles indicate ^{15}N-labeled nitrogens. KIC, α-ketoisocaproate; NEAAs, non-essential amino acids; TCA, tricarboxylic acid.

(F-H) Heatmap showing the relative labeling ion count changes detected by LC-MS analysis of TCA cycle metabolites (F), labeling amino acids (G) and labeling nucleotides (H) in MMC6 cells upon *METTL16* depletion.

(I) Relative proliferation rate changes of MMC6 cells upon *METTL16* KO in the BCAA-free medium (mean ± SD, n = 3 independent experiments).

(J) Validation of expression of METTL16, BCAT1 and BCAT2 in MMC6 cells after transduction with indicated lentiviruses via Western blotting.

(K-M) The effects of BCAT1 and BCAT2 overexpression on cell proliferation (K and L) and apoptosis (M) in MMC6 cells upon *METTL16* KO (mean ± SD, n = 3 independent experiments).

(N, O) Seahorse assays displaying the effects of forced expression of BCAT1 and BCAT2 on restoring OCR in MMC6 cells upon *METTL16* KO (mean ± SD, n = 4 independent experiments).

Statistical analysis: One-way ANOVA (A, C, D, and M); Two-way ANOVA (K and L); Unpaired t test (I). ns, not significant; *p < 0.05; **p < 0.01; ***p < 0.001. See also Figure S7.

KEY RESOURCES TABLE

REAGENT or RESOURCE	SOURCE	IDENTIFIER
Antibodies		
m^6A (N6-methyladenosine) antibody	Synaptic Systems	Cat# 202003; RRID: AB_2279214
Anti-METTL16 antibody	Bethyl Laboratories	Cat# A304-192A; RRID: AB_2620389
Anti-METTL16 antibody	Sigma-Aldrich	Cat# HPA020352
Anti-BCAT1 antibody	OriGene	Cat# TA504360, RRID: AB_11126287
Anti-BCAT2 antibody	Proteintech	Cat# 16417-1-AP, RRID: AB_10792411
Anti-LARS1 antibody	Proteintech	Cat# 21146-1-AP, RRID:AB_10733878
beta-Actin (8H10D10) Mouse mAb	Cell Signaling Technology	Cat# 3700, RRID: AB_2242334
Anti-vinculin Antibody	Santa Cruz Biotechnology	Cat# sc-25336; RRID: AB_628438
Monoclonal ANTI-FLAG M2 antibody	Sigma-Aldrich	Cat# F3165; RRID: AB_259529
Normal Mouse IgG control antibody	Millipore	Cat# 12-371; RRID: AB_145840
Goat anti-rabbit IgG H&L (HRP)	Abcam	Cat# ab6721; RRID: AB_955447
Goat anti-mouse IgG H&L (HRP)	Abcam	Cat# ab6789; RRID: AB_955439
Anti-Human CD45 BV786	BD Horizon	Cat# 563716; RRID: AB_2716864
Anti-Human CD34 FITC	eBioscience	Cat# 11-0349-42; RRID: AB_1518732
Anti-Puromycin antibody	EMD Millipore	Cat# MABE343; RRID: AB_2566826
Anti-rabbit IgG (H+L), F(ab')2 Fragment (Alexa Fluor 555 Conjugate)	Cell Signaling Technology	Cat# 4413S; RRID: AB_10694110
Anti-Human CD11b PE	eBioscience	Cat# 12-0118-42; RRID: AB_2043799
Anti-Human CD14 APC	eBioscience	Cat# 17-0149-42; RRID: AB_10669167
Anti-Mouse Lineage marks eFlour™ 450	eBioscience	Cat# 88-7772-72, RRID: AB_10426799
Anti-Mouse C-Kit APC	eBioscience	Cat# 17-1171-82, RRID: AB_469431
Anti-Mouse Sca-1 PE	eBioscience	Cat# 12-5981-82, RRID: AB_466086
Anti-Mouse CD16/32 APC/Cyanine7	BioLegend	Cat# 156612, RRID: AB_2800710
Anti-Mouse CD34 PE/Cyanine7	BioLegend	Cat# 119326, RRID: AB_2716078
Anti-Mouse CD150 PerCP-eFluor™ 710	Thermo Scientific	Cat# 46-1502-82, RRID:AB_10597740
Anti-Mouse CD48 FITC	eBioscience	Cat# 11-0481-82, RRID: AB_465077
Anti-Mouse CD3 APC	BioLegend	Cat# 100236, RRID: AB_2561456
Anti-Mouse B220 APC-Cyanine7	BD Bioscience	Cat# 561102, RRID: AB_10561687
Anti-Mouse Ter119 V450	BD Bioscience	Cat# BDB560504, RRID: AB_10563222
Anti-Mouse CD11b PerCP-Cyanine5.5	eBioscience	Cat# 45-0112-82, RRID: AB_953558
Anti-Mouse Gr1 PE	eBioscience	Cat# 12-5931-81, RRID: AB_466044
Anti-Mouse CD11b APC	eBioscience	Cat# 50-112-3031
Anti-Mouse CD45.2 APC	eBioscience	Cat# 17-0454-82; RRID: AB_469400
Anti-Mouse CD45.2 FITC	eBioscience	Cat# 109805, RRID:AB_313443
Anti-Mouse CD45.1 PE	eBioscience	Catalog # 12-0453-82 RRID: AB_465675
Gr-1-Biotin	eBioscience	Cat# 130-101-894, clone RB6-8C5
CD11b-Biotin	eBioscience	Cat# 130-098-582

REAGENT or RESOURCE	SOURCE	IDENTIFIER
Bacterial and virus strains		
Stbl3 E. coli	ThermoFisher	Cat# C7373-03
Biological samples		
Cord blood sample	StemCyte	N/A
Chemicals, peptides, and recombinant proteins		
Hexadimethrine bromide (Polybrene)	Sigma-Aldrich	Cat# H9268; CAS: 28728-55-4
Puromycin dihydrochloride	Sigma-Aldrich	Cat# P8833; CAS: 58-58-2
Hygromycin B Gold	Invivogen	Cat# ant-hg-1; CAS: 1282-04-9
Blasticidin	Invivogen	Cat# ant-bl-05
G418 Sulfate	Thermo Fisher Scientific	Cat# 10131027; CAS: 108321-42-2
Poly(I:C)	R&D systems	Cat# 4287/10
RetroNectin	Sigma-Aldrich	Cat# T202
L-Glutamine (200mM)	Thermo Fisher Scientific	Cat# 25030-081
Ammonium Chloride Solution	STEMCELL Technologies	Cat# 07850
MEM Non-Essential Amino Acids Solution (100x)	Thermo Fisher Scientific	Cat# 11-140-050
Sodium Pyruvate (100mM)	Thermo Fisher Scientific	Cat# 11360-070
Insulin, human recombinant zinc solution	Thermo Fisher Scientific	Cat# 12585014
Penicillin Streptomycin	Thermo Fisher Scientific	Cat# 15-140-122
Plasmocin prophylactic	Invivogen	Cat# ant-mpp
X-tremeGENE™ HP DNA Transfection Reagent	Roche	Cat# 6366236001
RIPA Buffer	Sigma-Aldrich	Cat# R0278
Halt Phosphatase Inhibitor Cocktail	Thermo Fisher Scientific	Cat# 78420
Halt Protease Inhibitor Cocktail	Thermo Fisher Scientific	Cat# 78429
4 x Laemmli Sample Buffer	Bio-Rad	Cat# 1610747
Bio-Rad Protein Assay	Bio-Rad	Cat# 5000006
PageRuler™ Plus Prestained Protein Ladder	Thermo Fisher Scientific	Cat# 26620
Amersham ECL Prime Western BlottingDetection Reagent	GE Healthcare	Cat# 45-010-090
Pierce™ ECL Western Blotting Substrate	Thermo Fisher Scientific	Cat# PI32106
Ficoll Paque Plus	GE Healthcare	Cat# 17-1440-02
Ammonium Chloride Solution	STEMCELL Technologies	Cat# 07850
Recombinant Human M-CSF	PeproTech	Cat# 300-25
Recombinant Human GM-CSF	PeproTech	Cat# 300-03
Recombinant Human IL-6	PeproTech	Cat# 200-06
Recombinant Human IL-3	PeproTech	Cat# 200-03
Recombinant Human SCF	PeproTech	Cat# 300-07
Recombinant Human TPO	PeproTech	Cat# 300-18
Recombinant Human Flt3-Ligand	PeproTech	Cat# 300-19
Recombinant mouse IL-3	PeproTech	Cat# 213-13
Recombinant mouse IL-7	eBiosciences	Cat# 14-8071-80

REAGENT or RESOURCE	SOURCE	IDENTIFIER
Recombinant murine Flt-3 ligand	PeproTech	Cat# 250-31L
Recombinant mouse SCF	PeproTech	Cat# 250-03
Recombinant murine GM-CSF	PeproTech	Cat# 315-03
ColonyGEL-Mouse Base Medium	Reachbio	Cat# 1201
ColonyGEL ⁻Human Base Medium	Reachbio	Cat# 1101
FastDigest NotI	Thermo Fisher Scientific	Cat# FD0595
FastDigest XbaI	Thermo Fisher Scientific	Cat# FD0684
FastDigest BamHI	Thermo Fisher Scientific	Cat# FD0054
FastDigest MluI	Thermo Fisher Scientific	Cat# FD0564
Actinomycin D	Sigma-Aldrich	Cat#A9415; CAS: 50-76-0
DL-Dithiothreitol solution	Sigma-Aldrich	Cat# 3483-12-3 ; CAS: 3483-12-3
0.5M EDTA	Thermo Fisher Scientific	Cat# 15575020
Paraformaldehyde Solution	Fisher scientific	Cat# AAJ19943K2
Wright-Giemsa Stain	Polysciences	Cat# 24985
Wright-Giemsa Stain/Buffer	Polysciences	Cat# 24984
Pierce Protein A/G Magnetic Beads	Thermo Fisher Scientific	Cat# 88803
D-Luciferin Firefly, potassium salt	Goldbio	Cat# LUCK; CAS: 115144-35-9
Platinum™ SuperFi II DNA Polymerase	Thermo Fisher Scientific	Cat# 12361010
S-(5′-Adenosyl)-L-methionine chloride dihydrochloride (SAM)	Sigma-Aldrich	Cat# A7007; CAS: 86867-01-8
Recombinant METTL16 protein	Active Motif	Cat# 81085
RNaseOUT Recombinant Ribonuclease Inhibitor	Thermo Fisher Scientific	Cat# 10777019
N6-Methyladenosine 5'-monophosphate (sodium salt)	Cayman Chemical Company	Cat# 23382; CAS: 81921-35-9
N6-Methyladenosine-d3	Toronto Research Chemicals	Cat# M275897; CAS: 139896-43-8
DNase I, RNase-free (1 U/μL)	Thermo Fisher Scientific	Cat# EN0521
Proteinase K	Thermo Fisher Scientific	Cat# EO0492
$^{13}C_6$, $^{15}N_1$-Leucine	CortecNet	Cat# CCN1600P01
RPMI 1640 Medium, 1X Liq., w/o L-Glutamine and L-Leucine	MP Biomedicals	Cat# ICN1629149
Critical commercial assays		
APC Annexin V Apoptosis Detection Kit	eBiosciences	Cat#88-8007-74
CellTiter 96 Non-Radioactive Cell Proliferation Assay	Promega	Cat#G4100
DNA Ligation Kit	Takara Bio	Cat# 6023
In-Fusion HD Cloning Plus CE Cat#	Takara	Cat# 638916
PCR Mycoplasma Detection Kit	Applied Biological Materials	Cat# G238
DNeasy Blood & Tissue Kit	QIAGEN	Cat# 69506
Dynabeads mRNA DIRECT Purification Kit	Thermo Fisher Scientific	Cat# 61011
CD34 MicroBead Kit, human	Miltenyi Biotec	Cat# 130-046-702
Lineage Cell Depletion Kit	Miltenyi Biotec	Cat#130-090-858
RNA Clean & Concentrator-5	Zymo Research	Cat# R1014

REAGENT or RESOURCE	SOURCE	IDENTIFIER
QIAGEN Plasmid Mini Kit	Qiagen	Cat# 12125
PolyATract mRNA isolation system IV	Promega	Cat# Z5310
QuantiTect Reverse Transcription Kit	Qiagen	Cat# 205314
Maxima SYBR Green qPCR Master Mix	Thermo Fisher Scientific	Cat# K0253
SuperScript™ III First-Strand Synthesis System	Invitrogen	Cat# 18080051
MEGAscript™ T7 kit	Invitrogen	Cat# AM1333
MEGAclear™ Transcription Clean-Up Kit	Invitrogen	Cat# AM1908
Seahorse XF Cell Mito Stress Test Kit	Agilent Technologies	Cat# 103015-100
Branched Chain Amino Acid Kit	Sigma-Aldrich	Cat# MAK003
Deposited data		
m^6A-seq (Raw and analyzed data)	This manuscript	GSE189995
RNA-seq (Raw and analyzed data)	This manuscript	GSE190044
Experimental models: Cell lines		
THP1	ATCC	TIB-202; RRID: CVCL_0006
NB4	DSMZ	ACC-207; RRID: CVCL_0005
HL-60	ATCC	CCL-240; RRID: CVCL_A794
NOMO-1	DSMZ	ACC-542; RRID: CVCL_1609
MOLM-13	DSMZ	ACC-554; RRID: CVCL_2119
HEL	ATCC	CCL-2
ML-2	DSMZ	ACC-15; RRID: CVCL_1418
Kasumi-1	ATCC	CRL-2724; RRID: CVCL_0589
OCI-AML3	Dr Ling Li (City of Hope, Duarte, CA)	N/A
MONOMAC6	DSMZ	ACC-124; RRID: CVCL_1426
KG-1a	ATCC	CCL-246.1
MA9.3ITD	A gift from Dr. James Mulloy	N/A
OP9	ATCC	CRL-2749; RRID: CVCL_4398
HEK293T	ATCC	CRL-3216; RRID: CVCL_0063
Experimental models: Organisms/strains		
NRGS mouse	The Jackson Laboratory	*Cat# JAX:024099; RRID: IMSR_JAX:024099NCI
NCI B6-Ly5.1/Cr mouse	Charles river	Cat# CRL:564; RRID: IMSR_CRL:564
NCI C57BL/6 Mouse	Charles river	Cat# CRL:556; RRID: IMSR_CRL:556
B6.Mettl16$^{fl/fl}$	Cyagen Biosciences	N/A
B6.Cg-Tg(Mx1-cre)1Cgn/J	The Jackson Laboratory	Strain #:003556 RRID:IMSR_JAX:003556
Oligonucleotides		
Primers for Real-time PCR, see Table S3	Integrated DNA Technologies (IDT)	N/A
Recombinant DNA		

REAGENT or RESOURCE	SOURCE	IDENTIFIER
pcDNA3-METTL16-WT	A gift from Dr. Nicholas K. Conrad	N/A
pcDNA3-METTL16-PP185/186AA	A gift from Dr. Nicholas K. Conrad	N/A
pcDNA3-METTL16-F187G	A gift from Dr. Nicholas K. Conrad	N/A
pMIRNA1-3xFlag-METTL16	This paper	N/A
pMIRNA1-METTL16-PP185/186AA	This paper	N/A
pMIRNA1-METTL16-F187G	This paper	N/A
pMIRNA1-3xFlag-METTL16-MUT1	This paper	N/A
pMIRNA1-3xFlag-METTL16-MUT2	This paper	N/A
pMIRNA1-METTL16-PP185/186AA-MUT1	This paper	N/A
pMIRNA1-METTL16-F187G MUT1	This paper	N/A
pSIN4-BCAT1	This paper	N/A
pMIRNA1-BCAT2	This paper	N/A
pLenti CMV Puro LUC (w168-1)	[60]	Addgene plasmid # 17477; RRID: Addgene_17477
pMD2.G	A gift from Dr. Didier Trono	Addgene plasmid # 12259; RRID: Addgene_12259
psPAX2	A gift from Didier Trono	Addgene plasmid # 12260; RRID: Addgene_12260
pLKO.1 puro	[61]	Addgene plasmid # 8453; RRID: Addgene_8453
pLKO.1-shMETTL16-1	This paper	N/A
pLKO.1-shMETTL16-2	This paper	N/A
pLKO.1-shMettl16-1	This paper	N/A
pLKO.1-shMettl16-2	This paper	N/A
pLKO.1-shYTHDC1-1	This paper	N/A
pLKO.1-shYTHDC1-2	This paper	N/A
pLKO.1-shIGF2BP2-1	This paper	N/A
pLKO.1-shIGF2BP2-2	This paper	N/A
lentiGuide-hygro	[62]	Addgene plasmid # 104991; RRID: Addgene_104991
lentiGuide-hygro-sgMETTL16-1	This paper	N/A
lentiGuide-hygro-sgMETTL16-2	This paper	N/A
lentiCas9-Blast	[63]	Addgene plasmid # 52962; RRID: Addgene_52962
MSCV-MLL-AF9-Neo	A gift from Dr. Michael Thirman	N/A
pCL-Eco	[64]	Addgene plasmid # 12371; RRID: Addgene_12371
Software and algorithms		
GraphPad Prism 8	GraphPad	https://www.graphpad.com/scientific-software/prism/
RSEM-1.2.31	[65]	https://deweylab.github.io/RSEM/

REAGENT or RESOURCE	SOURCE	IDENTIFIER
STAR 2.7	66	https://github.com/alexdobin/STAR
GSEA 4.2.0	50	https://www.gsea-msigdb.org/gsea/index.jsp